JOURNAL OF THE EXPERIMENTAL ANALYSIS OF BEHAVIOR 2008, **90,** 363–386 NUMBER 3 (NOVEMBER)

AN ANALYTIC FORM FOR THE INTERRESPONSE TIME ANALYSIS OF SHULL, GAYNOR, AND GRIMES WITH APPLICATIONS AND EXTENSIONS

ROBERT KESSEL AND ROBERT L. LUCKE

NAVAL RESEARCH LABORATORY

Shull, Gaynor and Grimes advanced a model for interresponse time distribution using probabilistic cycling between a higher-rate and a lower-rate response process. Both response processes are assumed to be random in time with a constant rate. The cycling between the two processes is assumed to have a constant transition probability that is independent of bout length. This report develops an analytic form of the model which has a natural parametrization for a higher-rate within-bout responding and a lower-rate visit-initiation responding. The analytic form provides a convenient basis for both a nonlinear least-squares data reduction technique to estimate the model's parameters and Monte Carlo simulations of the model. In addition, the analytic formulation is extended to both a refractory period for the rats' behavior and, separately, the strongly-banded behavior seen with pigeons.

Key words: IRT distributions, Monte Carlo simulation, pigeon IRT banding

Shull, Gaynor and Grimes (2001) used a state diagram representation for their elegant model for interresponse time (IRT) distributions. The core structure in their model is the assertion that the measured response population is generated by transitions between two separate and independent source populations:

- a long IRT component associated with the visit initiation time between bouts of operant behavior,
- a short IRT component associated with bouts of operant behavior.

While the state diagram's transitions circumscribe how these two populations may contribute, definitions of the two populations are also required. Shull et al. (2001) addressed this issue by assuming that both are random processes with uniform probability densities in time. Their article also dealt with two methodical matters that have more to do with reducing the experiment's data than the model itself. First, the authors used a log-survivor plot to compactly present the IRT population. Perhaps because a log-survivor plot highlights the IRT component forms posited by Shull et al. so clearly, its use has become convolved with the model itself. In fact, a log-survivor analysis is not required by their model and conditions do exist where its use can obscure the behavior processes. In addition to finding a particularly good visualization technique, they combined their model with their data collection hardware as a technique to extract these probability distribution parameters from an obtained IRT distribution. With the combination of their model and a well suited data reduction technique, Shull et al. then compared measured IRT distribution of rats against the model's predicted form and found reasonable agreement. Further, they determined some of the experimental variables that control the two components.

In subsequent articles Shull and his coauthors explored both a broader set of experimental conditions where the model is applicable and the conditions governing the probability distribution parameters. Shull, Gaynor, and Grimes (2002) studied relative resistance to change of the response distribution components. Shull and Grimes (2003) gave the effects of changing the response required of the rats from the original nose

The authors gratefully acknowledge the contributions of: Bill Palya for many helpful discussions while drafting this article; both Bill Palya and Matt Bowers for allowing unfettered access to E48's data, preliminary analyses and plots, and their article in pre-print; Don Walter for extracting and reformatting the E48 data files into an easily-used form, and Richard Shull for Rat C1's IRT data from Shull, Grimes, and Bennett (2004).

Address correspondence to Robert Kessel, Electro-Optics Technology Section, Code 8123, Naval Research Laboratory, Washington, D.C. 20375-5354(kessel@ncst.nrl.navy.mil). The software used in preparing this report is available from the JSU/SEBAC program archive at /www.jsu.edu/depart/psychology/sebac/analytic-form/. Also available as part of the web-appendix is a derivation of the exponential form for the inter-event intervals of a Poisson process.

doi: 10.1901/jeab.2008.90-363

poke to a lever press. By and large, the lever press behavior had the same characteristics as nose poking, with the differences confined to quantitative changes. For example, a lower rate for the within-bout responding resulted in a more rounded transition in the IRT distributions seen with lever pressing when compared to nose poking. Shull, Grimes, and Bennett (2004) presented a more detailed study of how the individual component parameters are affected in steady-state by overall rate on a variable-interval (VI) schedule, changes in the VI schedule, and the inclusion of a small variable-ratio requirement. The article also suggested a way to tie the within-bout and visit-initiation responding to time allocation matching. Shull (2004) measured the control deprivation level has upon the individual component parameters – deprivation primarily affects the visit-initiation rate. Starting with Shull and Grimes (2003), the probability distribution parameters estimation used weighted non-linear least squares implemented in SigmaPlot. This refined data analysis stemmed from a related Excel optimization application developed by Killeen (2003). Killeen's Excel application, itself, followed from a modified version of Shull et al.'s state diagram (Killeen, Hall, Reilly, & Kettle; 2002).

At least one alternative representation of the Shull, Gaynor and Grimes (2001) model is possible. This report reframes the Shull et al. model by expressing it in an analytic form. It is important to note that use of a state diagram provides a sufficient description in a heuristic sense, but it can be unwieldy in some circumstances. An analytic form lifts some limitations that are not inherent to the model. Unlike its initial definition via a narrative and a state diagram, or Killeen et al.'s (2002) closely related representation via machines, an analytic representation simplifies study of the model's characteristics. For example, issues of stability and precision that become important during data reduction can be resolved with reasonable clarity. Further, extensions of Shull et al.'s model to other types of organisms and behavior are far simpler once an analytic form is defined. Additionally, specific substitutions for individual elements have a natural setting.

The present report opens with the development of an analytic form of the Shull et al. model. First, we introduce the probability density functions that govern the model's components and the probabilistic cycling. These analytic expressions are then combined to yield the overall IRT probability density function. The second section of the report applies the resulting analytic expressions to the data reduction process. We set up the estimation of the model's parameters from IRT data as a non-linear least squares problem. We also consider the limitation imposed on data reduction processing by the sample size, using a Monte Carlo simulation. In the third section we extend Shull et al.'s model to include a refractory period or dead-time correction. In the fourth section, we consider replacing the uniform-in-time high rate process that has been used to describe the rats' nose-poking and lever pressing with the strongly-banded high rate process present in pigeon key pecks. This is done with reference to the experiments by Bowers, Zimmermann, and Palya (2003) and Bowers, Hill, and Palya (2008). We explore some aspects of the more complex behavioral repertoire of the pigeons using a second Monte Carlo simulation. This second Monte Carlo preserves the structure of the first, but components are modified to describe the pigeons. The article closes with a brief summary discussion.

ANALYTIC FORM OF THE SHULL, GAYNOR, AND GRIMES IRT MODEL

Shull, Gaynor, and Grimes (2001) presented their model of IRT distributions in an implicit version by employing the state diagram in their Figure 2 along with its caption and parts of the narrative descriptions in the introduction and their hardware simulation on pp. 249–250. It is relatively straightforward to put their model in an analytic form. Though our end point will be a set of equations, the starting point for this article's development is Shull et al.'s state diagram, shown in Figure 1. It is important to note at the outset that this state diagram implies a specific and very local description of how the supported behavior can unfold in time. By itself, however, the state diagram does not have an inherent time scale or cadence. The time scale is determined by the transition probabilities one chooses to employ. In other words, Shull et al.'s model has its structural backbone fixed by the state diagram, yet it still

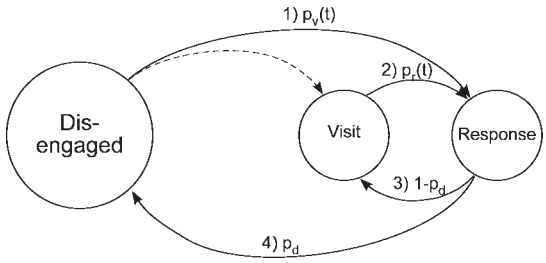

Fig. 1. A modified version of Shull et al.'s (2001) state diagram. The dashed arrow is present in the original, but is replaced here by transition 1, the solid arrow from the disengaged state to the response state. Transitions 1 and 2 have a deterministic endpoint at the response state, but are probabilistic in transition interval. Hence, the transition probabilities, $p_v(t)$ and $p_r(t)$, are written as functions of time. In contrast, transitions 3 and 4 that occur after a response are probabilistic only in end state, either remaining in the visit state or ending the bout of responses by a transition to the disengaged state. Hence, the probability, p_d, of disengaging after each response is discrete number.

derives considerable flexibility from the transition probabilities. As a matter of taxonomy, it seems fair to claim that so long as Figure 1 is preserved, one is using a Shull et al. model. The two extensions covered in later sections of this article are of this form – Figure 1 is preserved, but the transition probabilities differ from those originally used by Shull et al. Note that we have made one minor structural change in the state diagram. The original version of Figure 1 had a transition from the disengaged state to the visit state, shown as the dashed arrow. As a practical matter, the transition from the disengaged state is signaled in the data by a response. Consequently, our version of the state diagram has a direct transition, shown as a solid arrow, from the disengaged state to the response state. Only this transition is experimentally observable, the dashed-arrow transition is not.

In contrast to the state diagram's explicit form, Shull et al. (2001) defined the transitions between states in terms of their properties. To refine the definition of these transitions it is useful to consider how the model's transitions yield response sequences in terms of visit cycles. A short sample of the response sequence that follows from the Figure 1 state diagram is shown in Figure 2. Each cycle of the model contains an initial visit initiation period followed by a bout of n responses. Then the organism switches back to the disengaged state and the next cycle begins. Shull et al. presuppose that the visit-initiation period, the number of responses within a bout, and the within-bout IRTs all are random variables. As we noted above, a visit-initiation period ends with a response. Hence, we will drop the distinction between a visit-initiation period and a within-bout IRT and refer to the former as a visit-initiation IRT. To formalize slightly, the Shull, et al. model for the supported behavior yields an IRT sequence that is the result of probabilistic cycling between distinct low-rate and high-rate random processes. The visit-initiation intervals from the low-rate process and the within-bout response intervals from the high-rate process constitute the complete population that make up the IRT distribution.

All that remains to reach an analytic form for Shull et al.'s (2001) model is the selection of some appropriate probability densities followed by a bit of assembly. Both low-rate visit-initiation and high-rate within-bout response processes shown by transitions 1 and 2 in Figure 1 have convenient descriptions in terms of time-dependent continuous probability densities. The probabilistic cycling between these two processes shown by transitions 3 and 4 in Figure 1, however, is defined by the time-independent disengagement probability p_d. Hence, the model's time scale is set entirely by transitions 1 and 2. It will prove useful to develop a discrete probability density for the number of responses per visit (cf. Equation 6) from the disengagement probability p_d. First, though, we will develop expressions for the continuous probability densities of the two response processes.

Shull et al. (2001), and later Killeen et al. (2002), specified the visit-initiation and within-bout response intervals by introducing an ancillary very high rate discrete time base. By sampling a discrete probability against a fixed threshold far faster than the average within-bout IRT or visit-initiation IRT, Shull et al. effectively asserted that, for the organism and behavior in their studies, both the visit initiation and within-bout responses are randomly distributed in time at a constant average rate. In formal terminology, they were asserting that both the long and short IRT components are Poisson processes, which can be conveniently described by continuous probability densities. In fact, taking the limit as the

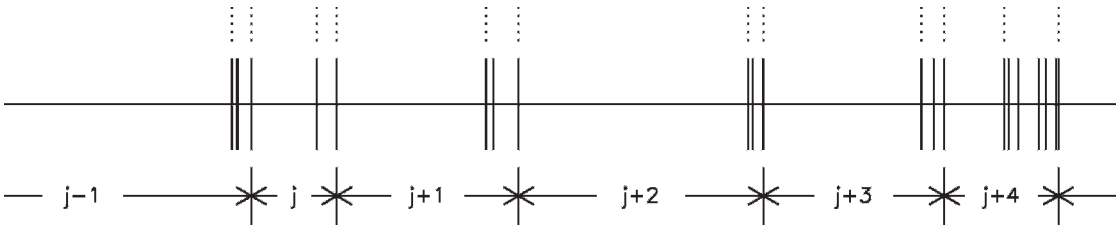

Fig. 2. A few cycles' response times about the j^{th} bout for Shull et al.'s (2001) model. The cycles are labeled below and run continuously. The bouts are marked off with dashed lines above. The $j-1$ bout has 3 responses, the j bout has 2 response, etc.

ancillary discrete time base interval approaches zero is a standard technique to derive the inter-event spacing for a Poisson process. Furthermore, it is simpler to extend Shull et al.'s model with continuous probability densities, and that is the approach adopted here.

The separations between events governed by a Poisson process have an exponential distribution (Enge, 1966; also this report's web-appendix[see Author Note]). The appropriate Poisson probability density functions for the visit-initiation and within-bout IRTs are both given in the standard form as:

$$p_v(t) = \frac{1}{\tau_v} e^{-t/\tau_v} \tag{1}$$

and

$$p_r(t) = \frac{1}{\tau_r} e^{-t/\tau_r}, \tag{2}$$

which differ only by the time scale parameters for visit-initiation responding, τ_v, and within-bout responding, τ_r. A clear experimental finding by Shull et al. (2001) is that for rats' nose pokes or lever presses $\tau_v \gg \tau_r$. Note that the assumption of constant-rate random distributions in time for both processes is not required by the cycling illustrated in Figure 1 – it is a second, independent, element of Shull et al.'s model. Equations 1 and 2 give an explicit form for this second element of the Shull et al. model.

The number of responses within a bout is determined in Shull et al.'s (2001) model by the probability p_d of ending a bout after a response. This is the point where a discrete probability density enters the model. The probabilities for a bout to end with one, two, or three responses are

$$p_e(1) = p_d, \tag{3}$$

$$p_e(2) = (1 - p_d)p_d, \tag{4}$$

and

$$p_e(3) = (1 - p_d)^2 p_d, \tag{5}$$

respectively. In general, the discrete probability density function for a given cycle to end after n responses is

$$p_e(n) = (1 - p_d)^{n-1} p_d. \tag{6}$$

Equation 6, when combined with Equations 1 and 2, provides the analytic form of the Shull, et al. model. With these three expressions, the model can be used to describe the local (or fine) structure of the response dynamics. This local form of the Shull et al. model has two immediate uses. First, the equations are the basis for the Monte Carlo simulation described in Appendix A. Second, one can use these equations to calculate the more molar, time-averaged property used by Shull and his coworkers: the IRT distribution.

(One thing the Shull et al. (2001) model does not include is a relationship to the reinforcement schedule which is supporting the responding. As discussed in both the original Shull et al. (2001) article and subsequently by Shull and Grimes (2003), ascertaining the dependence of τ_v, τ_r, and p_d upon characteristics of the reinforcement conditions is an experimental question.)

The overall IRT probability density function follows fairly promptly by combining Equations 1, 2, and 6. It is a matter of summing contributions from the two IRT populations weighted by their relative probabilities. The average number of responses in a single cycle of the model is given by

$$\bar{n} = \sum n p_e(n), \tag{7}$$

$$= p_d + 2(1 - p_d)p_d + 3(1 - p_d)^2 p_d + \cdots + n(1 - p_d)^{n-1} p_d + \cdots, \quad (8)$$

$$= p_d\left[1 + 2(1 - p_d) + 3(1 - p_d)^2 + \cdots + n(1 - p_d)^{n-1} + \cdots\right]. \quad (9)$$

Using the standard series expansion

$$\frac{1}{(1 - x)^2} = \sum_{n=0}^{\infty} (n + 1)x^n = 1 + 2x + 3x^2 + 4x^3 + \cdots, \quad (10)$$

(Peirce, 1929) which is valid for $0 \leq x < 1$, simplifies Equation 9 to

$$\bar{n} = p_d \frac{1}{[1 - (1 - p_d)]^2} = p_d \frac{1}{p_d^2} = \frac{1}{p_d}. \quad (11)$$

Since all bouts are preceded with a single visit-initiation IRT, the fraction of the responses due to visit initiation is

$$F_v = \frac{1}{\bar{n}} = p_d. \quad (12)$$

The fraction that are not due to a visit initiation is therefore

$$F_r = 1 - F_v = 1 - p_d. \quad (13)$$

The overall IRT probability distribution is independent of the order of the IRT sequence present in Figure 2. Consequently, the net probability density of the IRTs is a weighted sum of $p_v(t)$ and $p_r(t)$ which we write as

$$p_{\mathrm{IRT}}(t) = F_v p_v(t) + F_r p_r(t). \quad (14)$$

Equation 14 gives the net probability density of the IRTs as the sum of the two contributing densities, weighted by the probability that a particular IRT is chosen from either of them. By itself, Equation 14 is a simple assertion of a two-population-based IRT model; it is less well defined than Shull et al.'s (2001) model as shown in Figure 1. In contrast, the state diagram, the asserted Poisson distribution for the visit-initiation and within-bout IRTs, and the probabilistic cycling of Shull et al.'s model lead to the precise expressions for $p_v(t)$, $p_r(t)$, $\bar{n}$, and a specific form

$$p_{\mathrm{IRT}}(t; \tau_v, \tau_r, p_d) = \frac{p_d}{\tau_v} e^{-t/\tau_v} + \frac{1 - p_d}{\tau_r} e^{-t/\tau_r} \quad (15)$$

upon substitution of the right sides of Equations 1, 2, 12, and 13. The augmentation of the argument list to include τ_v, τ_r, and p_d as one moves from Equation 14 to Equation 15 reflects the form of the model. The semicolon is a common notation to split the argument list into the single variable for the IRT probability density axis, t, and a set of three control parameters. For steady-state behavior after acquisition dynamics have faded, one expects τ_v, τ_r, and p_d to have reached constant values. In other words, the Shull, et al. model generates the family of IRT distributions that satisfy Equation 15, while the τ_v, τ_r, and p_d value set selects a member distribution applicable in a given situation.

It is of importance that Equation 15 is a probability density function, not a probability. As such, Equation 15 gives the probability density for an IRT to take an exact value. However, an exact outcome for a continuous random variable such as an IRT value only occurs with a vanishingly small probability. One obtains a finite probability by considering a measurable range of IRT values. Formally one integrates $p_{\mathrm{IRT}}(t; \tau_v, \tau_r, p_d)$ over the range as

$$P_{\mathrm{IRT}}(t_1, t_2; \tau_v, \tau_r, p_d) = \int_{t_1}^{t_2} p_{\mathrm{IRT}}(t; \tau_v, \tau_r, p_d)\, dt, \quad (16)$$

$$= p_d\left[e^{-t_1/\tau_v} - e^{-t_2/\tau_v}\right] + (1 - p_d)\left[e^{-t_1/\tau_r} - e^{-t_2/\tau_r}\right] \quad (17)$$

to get the probability of an IRT within that range.

Figure 3 shows some examples of Equation 15's IRT probability density function. One consequence of using a probability density is that the curve for p_{IRT} in Figure 3 with $\tau_v = 10$, $\tau_r = 0.5$, and $p_d = 0.2$ exceeds 1.0 for $t < 0.2375$. When integrated over the small interval between 0 and 0.2375, the resulting probability is less than 1. A more important aspect of developing Shull et al.'s (2001) model in terms of probability densities con-

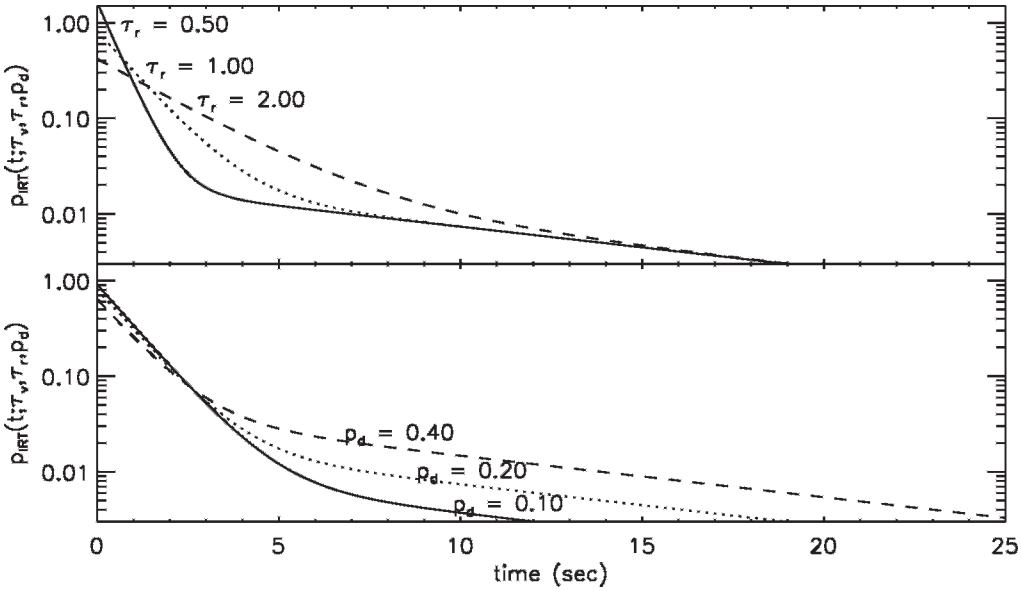

Fig. 3. $p_{\mathrm{IRT}}(t;\, \tau_v,\, \tau_r,\, p_d)$ with fixed values of $\tau_v = 10.0$ s and $p_d = 0.2$ and varying $\tau_r = 0.5$, 1.0, and, 2.0 s (top panel). $p_{\mathrm{IRT}}(t;\, \tau_v,\, \tau_r,\, p_d)$ with fixed values of $\tau_v = 10.0$ s and $\tau_r = 1.0$ s and varying $p_d = 0.1$, 0.2, and, 0.4 (bottom panel).

cerns testing it against experimental observations. Any comparison against real data requires integrating over an appropriate range of p_{IRT} values and Equation 17 will be used later for this purpose. Shull et al. used a second such integral over p_{IRT}: the survivor fraction. The conversion of an IRT probability density function to survivor fraction is given by the expression:

$$\mathrm{surv}_{\mathrm{IRT}}(t;\tau_v,\tau_r,p_d) = \int_t^{\infty} p_{\mathrm{IRT}}(t';\tau_v,\tau_r,p_d)\,dt', \tag{18}$$

$$= p_d e^{-t/\tau_v} + (1 - p_d)e^{-t/\tau_r}. \tag{19}$$

Figure 4 shows Equation 19 plotted on semilog axes (i.e. a log-survivor plot) for the same parameters used to generate Figure 3. Figure 4 recovers the two-limbed, or broken stick, form shown in Shull et al.'s Figure 3 (2001), though the continuous evaluation possible with an analytic expression yields smoother curves. For completeness, also shown in Figure 4 are extrapolations back to zero time of the visit-initiation populations. As follows from the first term in Equation 19, $p_d\, e^{-t/\tau_v}$, extrapolating an intercept of $\mathrm{surv}_{\mathrm{IRT}}$ $(t;\, \tau_v,\, \tau_r,\, p_d)$ from the IRTs that satisfy $t \gg \tau_r$ back to zero gives p_d. This formally recovers the other result given in Shull et al.'s Figure 3 – extrapolating to $t = 0$ in log-survivor coordinates yields p_d. Finally, reaching Equation 19 from the state diagram and Equations 1, 2, and 6 is the constructive proof that Shull et al.'s Equation 2 (2003) and the equivalent expression in Killeen's Excel spreadsheet (2003) are the correct form required by the model.

To foreshadow the type of extensions to be considered later, the model developed by Shull and his colleagues can be made more flexible by allowing changes in the definitions of $p_v(t)$, $p_r(t)$, or p_d. The extension of this model to pigeons relaxes the constraint of a common form for Equations 1 and 2 by using two distinct probability density functions for $p_v(t)$ and $p_r(t)$. Similarly, a different model of how a bout ends would yield a different computation for F_v changing the forms of Equations 12 and 15. There are a myriad of behaviorally reasonable alternative models. As one example, some organisms may simply never exceed a maximum number of responses within a bout no matter how rich the schedule. This would truncate the series in Equation 8, somewhat reduce the value of $\bar{n}$, and change the extrapolated intercepts in Figure 4. As a second example, p_d could be

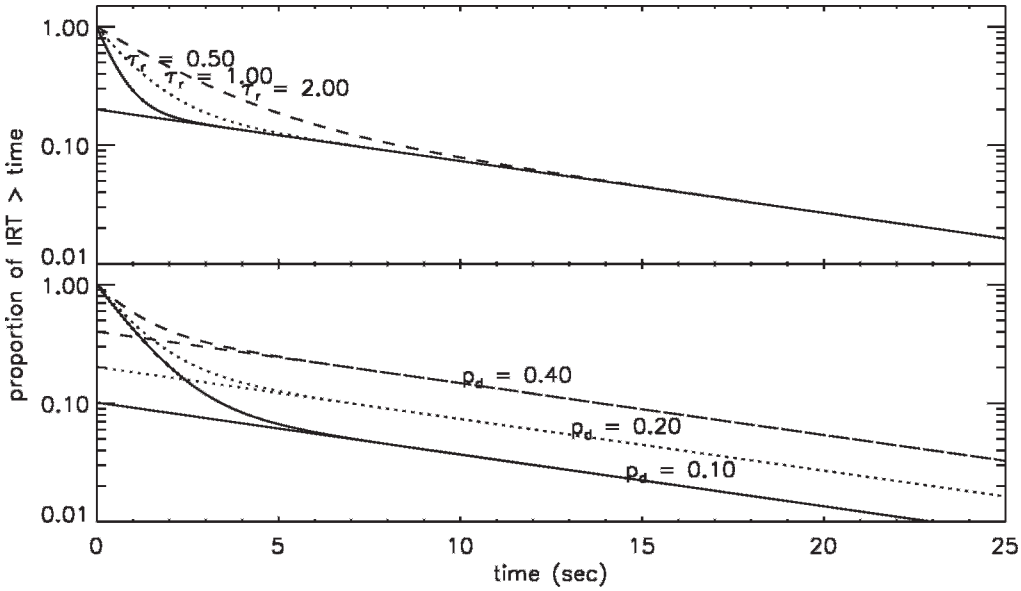

Fig. 4. Log-survivor plot of $\text{surv}_{\text{IRT}}(t; \tau_v, \tau_r, p_d)$ with fixed values of $\tau_v = 10.0$ s and $p_d = 0.2$ and varying $\tau_r = 0.5$, 1.0, and, 2.0 s (top panel). Log-survivor plot of $\text{surv}_{\text{IRT}}(t; \tau_v, \tau_r, p_d)$ with fixed values of $\tau_v = 10.0$ s and $\tau_r = 1.0$ s and varying $p_d = 0.1$, 0.2, and, 0.4 (bottom panel). Also shown in both panels are extrapolations to $t = 0$ of the visit-initiation populations.

made an increasing function of bout time which would change the detailed dynamics of the response sequences allowed.

APPLICATIONS OF THE ANALYTIC FORM

The immediate applications for Equation 15, along with the expressions leading to it and some derived from it, arise when comparing experimental data to the Shull et al. (2001) model. Either Equations 17 or 19 can serve as the basis for robust estimations of τ_v, τ_r, and p_d from experimental data. For example, Killeen's (2003) Excel spreadsheet is based on Equation 19. We will consider both forms. A somewhat more involved application is using Equations 1, 2, and 6 to write a Monte Carlo simulation of Shull *et al.*'s model. While such a simulation can be used in a variety of ways, we use it here to examine how the precision of parameter estimation depends upon data set size.

Non-linear Least Squares Estimates for τ_v, τ_r, and p_d from data

Estimation of τ_v, τ_r, and p_d from experimental data is a problem in non-linear least squares estimation (Killeen, 2003; Shull & Grimes, 2003). In our case, we choose to define the residuals required for such an estimation in two ways: first with respect to the IRT probability density function p_{IRT} via Equation 17, and second, with respect to the survivor fraction surv_{IRT} given by Equation 19. It will turn out not to matter which residual is used. We also depart from Killeen (2003) by weighting the least squares estimation with the residual variance and, to a lesser extent, from Shull and Grimes (2003) by using a weighting specifically derived for the least squares optimization in use.

To work from data, as opposed to exploring the properties of an analytic form (e.g. Figures 3 and 4), first requires a bit of preliminary processing. The IRT data are converted to a histogram where $N_{\text{IRT}}(t_i)$ is the number of IRTs in a bin about t_i. Next the data are converted into a normalized histogram of N bins as,

$$n_{\text{IRT}}(t_i) = \frac{N_{\text{IRT}}(t_i)}{\sum_{i=1}^{N} N_{\text{IRT}}(t_i)}, \qquad (20)$$

An important property of Poisson-distributed data is that the uncertainty of $N_{\text{IRT}}(t_i)$ for the bin about t_i is

$$\sigma_{N_{\mathrm{IRT}_i}} = \sqrt{N_{\mathrm{IRT}}(t_i)} \tag{21}$$

(Enge, 1966). Consequently, the uncertainty in $n_{\mathrm{IRT}}(t_i)$ is approximately

$$\sigma_{n_{\mathrm{IRT}_i}} = \frac{\sqrt{N_{\mathrm{IRT}}(t_i)}}{\sum_{i=1}^{N} N_{\mathrm{IRT}}(t_i)}, \tag{22}$$

since relative uncertainty in total number of IRTs, $\sqrt{\sum_{i=1}^{N} N_{\mathrm{IRT}}(t_i)}$, will be much smaller than the uncertainty in an individual bin. The analog to Equation 20 for the normalized survivor fraction when working with experimental data is the ratio of two sums over the histogram:

$$\widehat{\mathrm{surv}}_{\mathrm{IRT}}(t_i) = \frac{\sum_{j=i}^{N} N_{\mathrm{IRT}}(t_j)}{\sum_{i=1}^{N} N_{\mathrm{IRT}}(t_i)}, \tag{23}$$

where the ˆ superscript denotes a survivor fraction computed from data. Note that while Equation 18 is an analytic equivalent of Equation 23, it does not require the normalization present in Equation 23 because $p_{\mathrm{IRT}}(t; \tau_v, \tau_r, p_d)$ was constructed to have a normalization of 1 from the outset. The expression for the uncertainty in $\mathrm{surv}_{\mathrm{IRT}}(t_i)$ is

$$\sigma_{\mathrm{surv}_{\mathrm{IRT}_i}} = \frac{\sum_{j=i}^{N} N_{\mathrm{IRT}}(t_j)}{\sum_{i=1}^{N} N_{\mathrm{IRT}}(t_i)} \times \sqrt{1 \Big/ \left(\sum_{j=i}^{N} N_{\mathrm{IRT}}(t_j)\right) + 1 \Big/ \left(\sum_{i=1}^{N} N_{\mathrm{IRT}}(t_i)\right)} \tag{24}$$

(Bevington and Robinson, 2002, pp. 39–45). Equation 24 is somewhat more involved than Equation 22 since there are bins at low values of i where the sum in the numerator of Equation 23 will be of comparable size to the sum in the denominator.

One reduced chi-square expression appropriate for a weighted least-squares estimate of τ_v, τ_r, and p_d using the Equation 17 integral over the probability density is

$$\chi_v^2 = \frac{1}{N - n} \sum_{i=1}^{N} \frac{1}{\sigma^2_{n_{\mathrm{IRT}_i}}} \left(n_{\mathrm{IRT}}(t_i) - P_{\mathrm{IRT}}(t_i, t_{i+1}; \tau_v, \tau_r, p_d)\right)^2, \tag{25}$$

$$= \frac{1}{N - 3} \sum_{i=1}^{N} \frac{1}{\sigma^2_{n_{\mathrm{IRT}_i}}} \left(n_{\mathrm{IRT}}(t_i) - p_d\left[e^{-t_1/\tau_v} - e^{-t_2/\tau_v}\right] - (1 - p_d)\left[e^{-t_1/\tau_r} - e^{-t_2/\tau_r}\right]\right)^2, \tag{26}$$

where, in this case, $\nu = N - 3$ is the degrees of freedom and $\sigma^2_{n_{\mathrm{IRT}_i}}$ is the variance associated with the $i^{\underline{\mathrm{th}}}$ IRT residual $n_{\mathrm{IRT}}(t_i) - P_{\mathrm{IRT}}(t_i, t_{i+1}; \tau_v, \tau_r, p_d)$, as given by Equation 22. Note that the $1/\sigma^2_{n_{\mathrm{IRT}}i}$ factor is the weighting. Press, Flannery, Teukolsky, and Vetterling (1996) provide an implementation in both C and FORTRAN of the Levenberg-Marquardt algorithm, mrqmin, which will compute the least-squares best estimates for τ_v, τ_r, and p_d. Including a weighting factor like that given by Equation 22 is particularly important when the uncertainty varies significantly in magnitude. See Press et al.'s discussion on this point. Note that Shull et al.'s (2001) SigmaPlot routine uses the inverse weighting option to generate a similar effect within their data reduction. Commercial data analysis packages (e.g. IDL or Mathlab) have Levenberg-Marquardt routines based on Press et al. that are immediately applicable to Equation 26. The partial derivatives required in using the Levenberg-Marquardt algorithm are given in Appendix B. An alternative reduced chi-square expression for a weighted least-squares estimate based on the survivor fraction is

$$\chi_v^2 = \frac{1}{N - n} \sum_{i=1}^{N} \frac{1}{\sigma^2_{\mathrm{surv}_{\mathrm{IRT}_i}}} \left(\widehat{\mathrm{surv}}_{\mathrm{IRT}}(t_i) - \mathrm{surv}_{\mathrm{IRT}}(t; \tau_v, \tau_r, p_d)\right)^2, \tag{27}$$

$$= \frac{1}{N - 3} \sum_{i=1}^{N} \frac{1}{\sigma^2_{\mathrm{surv}_{\mathrm{IRT}_i}}} \left(\widehat{\mathrm{surv}}_{\mathrm{IRT}}(t_i) - p_d e^{-t/\tau_v} - (1 - p_d) e^{-t/\tau_r}\right)^2, \tag{28}$$

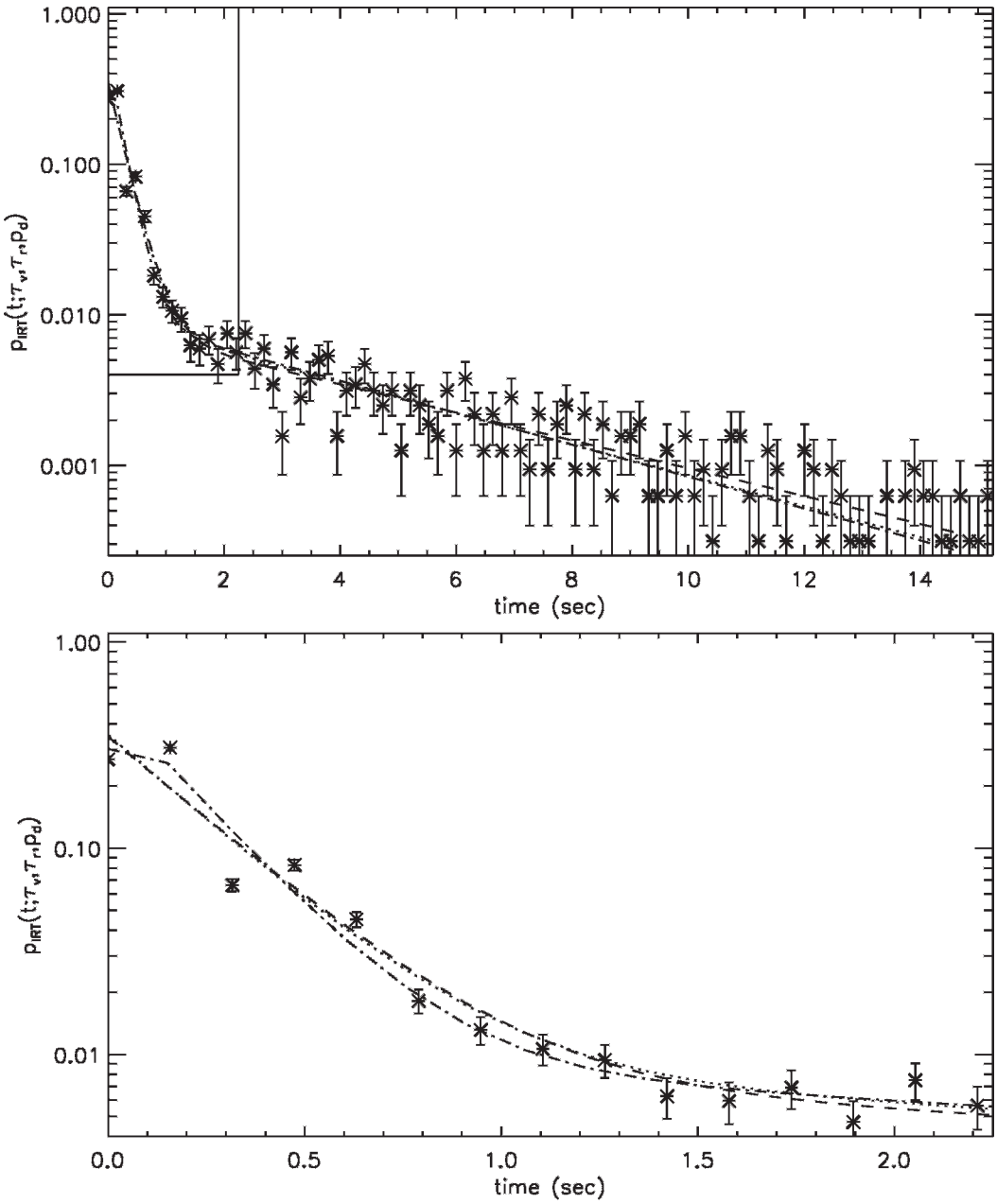

Fig. 5. IRT data from Shull et al.'s (2004) Rat C1 plotted as a normalized histogram with uncertainty brackets from Equation 22. The bottom panel shows subregion of the top panel within the box. The fit against P_{IRT} (Equations 17 and 26) is shown as a dashed curve. The fit against survivor fraction (Equations 19 and 28) is shown as a dotted curve. The survivor fraction fit with refractory period (Equations 38 and 39) is shown by the dash-dot curve.

The degrees of freedom are still given by $\nu = N - 3$. The variance $\sigma^2_{\mathrm{surv}_{\mathrm{IRT}_i}}$ of the $i^{\underline{\mathrm{th}}}$ survivor residual, $\widehat{\mathrm{surv}}_{\mathrm{IRT}}(t_i) - \mathrm{surv}_{\mathrm{IRT}}(t;\tau_v,\tau_r,p_d)$ is given by Equation 24. As with Equation 26, the least-squares best estimates for τ_v, τ_r, and p_d can be found with the Levenberg-Marquardt algorithm and the required partial derivatives are also given in Appendix B.

Table 1

Fit parameters for Shull *et al.*'s Rat C1.

	τ_v	τ_r	p_d	δ
P_{IRT} fit	4.69	0.266	0.244	
survivor fraction fit	4.22	0.257	0.250	
refractory survivor fraction fit	4.10	0.206	0.252	0.0539

Figure 5 shows an IRT data set for Rat C1 on a VI 60-s schedule (Shull, Grimes, & Bennett, 2004) after the data have been processed into a normalized histogram using Equation 20. Also shown are the uncertainty brackets for each histogram bin given by Equation 22. As the IRTs lengthen, the number of IRTs within a bin drops and, consequently, the relative uncertainty increases. It is this systematic variation in uncertainty that makes a weighted fit important. The dashed curve in Figure 5 is a Levenberg-Marquardt fit generated with Equation 26. The survivor fraction fit with Equation 28 estimates for τ_v, τ_r, and p_d result in the dotted curve in Figure 5. There is no obvious reason to prefer one fit over the other as both are faithful representations of the data in Figure 5. Table 1 gives the fit parameters for both the P_{IRT} and survivor fraction fits. We will address the modest difference in τ_v for the two fits below using the Monte Carlo simulation.

The use of semilog coordinates in Figure 5, as well as in Figures 3 and 4, is a good way to present the results. The efficacy of semilog coordinates for IRT data with exponential distributions (e.g. governed by Equation 15) occurs because an exponential becomes a straight line in semi-log coordinates. Since Shull et al.'s (2001) model has a pair of exponentials, one can, in many cases, easily discriminate between the within-bout and visit-initiation populations (e.g. in Figures 3, 4, and 5). Further, by its nature, it is usually easier to visually detect systematic departures from a straight line than from a curve. Consequently, one can efficiently inspect residuals from a number of experimental subjects as an initial check for a common and systematic departure from the model's predictions. In the present case with data from only the single subject, use of semilog coordinates suggests that for the shortest few IRT bins, as isolated in the bottom panel of Figure 5, both dashed and dotted fits do depart somewhat from the measured data. Despite the obvious utility of semilog and/or log-survivor coordinates, such plots, however, are not inherently part of Shull *et al.*'s model. The model is the Figure 1 state diagram, Equations 1, 2, and 6, and, if one is interested in IRT distributions, Equation 15. In fact, once one goes over to a full non-linear least-squares approach, the use of semi-log coordinates is not even part of the data reduction. Both Equations 26 and 28 are fit without using a semilog transformation. One can improve convergence of Equation 26's fit somewhat by using a variable, log-based, bin width, but it is not required for Figure 5.

Killeen's (2003) Excel application uses a different approach to estimate τ_v, τ_r, and p_d. Rather than process the IRT set, $\{\mathrm{IRT}_i\}$, into a histogram, they are sorted into increasing order with duplicates retained. As a notation for the sorted IRT set, we will use $\{\mathrm{IRT}_i^{\mathrm{sort}}\}$. Retaining duplicates is of significance for experimental data – finite timing resolution results in duplicates in Rat C1's IRT distribution. Killeen then set up an unweighted least-squares optimization problem for the entire sorted IRT list using the residual sum-squared expression

$$\chi^2 = \sum_{i=1}^{N} \left(surv\_frac\left[\mathrm{IRT}_i^{\mathrm{sort}}\right] - p_d e^{-t/\tau_v} - (1 - p_d) e^{-t/\tau_r} \right)^2. \tag{29}$$

The survivor fraction for the i^{th} sorted IRT is given by

$$surv\_frac\left[\mathrm{IRT}_i^{\mathrm{sort}}\right] = \frac{N - (i - 1)}{N}. \tag{30}$$

For duplicates within $\{\mathrm{IRT}_i^{\mathrm{sort}}\}$ Killeen set all their survivor fraction values to the value from the last ordinal position occupied by the duplicates. Equation 29's sum is then minimized with Excel's Solver which, in turn, employs a Generalized Reduced Gradient (GRG2) nonlinear optimization routine. As Excel's GRG2 routine is a proprietary code, the effect on the estimates for τ_v, τ_r, and p_d by the much greater prevalence of short IRT values or the duplicate entries is unknown.

Monte Carlo Tests of Sample Size Dependence

In the limit of an infinitely large data set and infinitely fine binning, $n_{\mathrm{IRT}}(t_i)$ goes to $p_{\mathrm{IRT}}(t_i;$

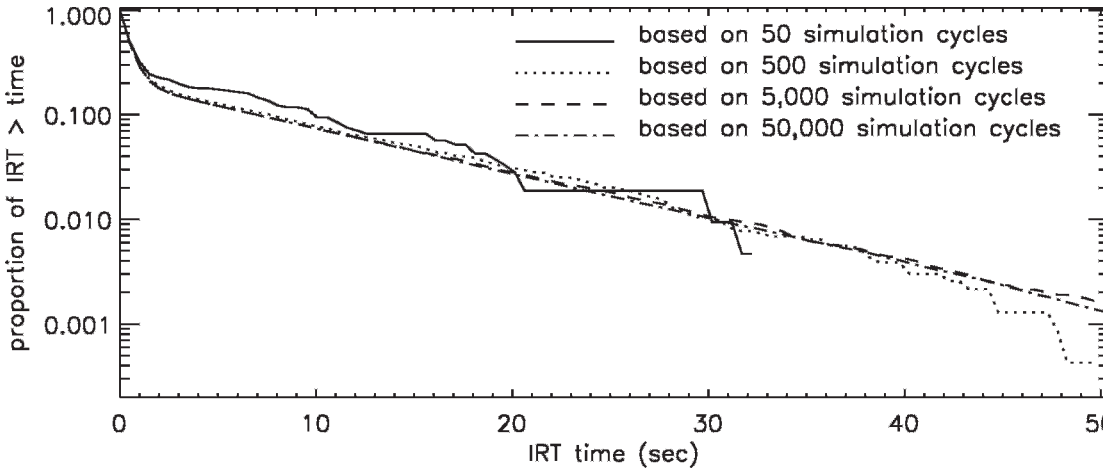

Fig. 6. Survivor fraction plots for 50, 500, 5,000 and 50,000 simulation cycles with τ_v = 10.0 s, τ_r = 0.5 s, and p_d = 0.2.

τ_v, τ_r, p_d). This leaves open the question of how quickly a finite data set will approach the limit. One method to gain such convergence information is to build a Monte Carlo simulation. Such a software emulation makes exploration of the model's sample-size dependence practicable. Equations 1, 2, and 6 are a convenient basis for a software Monte Carlo simulation of Shull et al.'s (2001) model. The Monte Carlo's sets of random numbers distributed according to Equations 1, 2, and 6 are generated from uniformly-distributed, floating-point, pseudo-random numbers in the range $0 < u < 1.0$ by a remapping that equates the cumulative probabilities. The details of the Monte Carlo and the analytic definitions for the remappings are given in Appendix A.

Figure 6 illustrates the convergence of a log-survivor plot as a function of the number of simulation cycles used. As might be expected, the curves generated from the histograms with Equation 23 become smoother as more simulation cycles are included. The curves also extend to greater multiples of τ_v as the comparatively rarer longer visit-initiation IRTs are generated by the simulation. Note that at the longer IRT values, the simulations for 50 and 500 cycles show a similar deficit in IRT number as is seen in Shull et al.'s results for steady-state behavior. Also note that the Monte Carlos' log-survivor curves are smoother towards the short IRT end. This reduction in the curves' fluctuations is the same effect as the narrowing of the uncertainty brackets at smaller IRT values noted for Figure 5. That the short IRT end of the distribution is better determined has a quantitative effect on the precision with which we can estimate τ_v, τ_r, and p_d.

To quantify the convergence, we use the fact that the Monte Carlo output has exactly the same form as an experimental IRT data set. Consequently, the same Levenberg-Marquardt fit routines used for Figure 5 are also applicable to Monte Carlo results. With appropriate control of the random number routine's seed values, one can generate multiple independent samples with the same number of simulation cycles. Figure 7 shows the convergence of τ_v, τ_r, and p_d as a function of the number of simulation cycles when fitting against the probability density. Figure 8 shows the corresponding convergence results for a survivor fraction fit. For either fit procedure, the fastest convergence in terms of relative uncertainty is in τ_r, followed fairly closely by p_d, and then noticeably lagged by τ_v. Between the two techniques, the survivor fraction has a somewhat faster convergence, particularly for τ_v's convergence. The differing rates of parameter convergence is of particular relevance to the behavioral momentum results (Shull, Gaynor, and Grimes; 2002). Even using group means, it is not clear that the sample sizes are large enough. Based on convergence seen Figures 7 and 8, these smaller IRT populations should yield τ_r and p_d estimates good to $\pm 2\%$, but the τ_v are, at best, $\pm 10\%$.

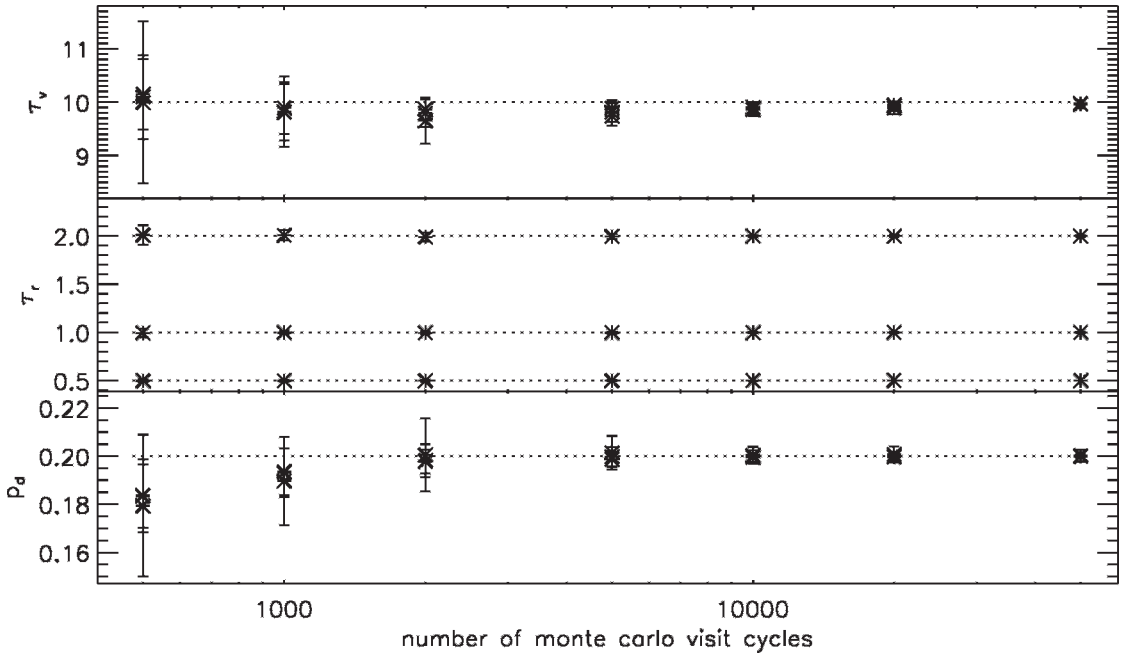

Fig. 7. Monte Carlo convergence tests of Equation 26's fit of P_{IRT} with fixed values of $\tau_v = 10.0$ s and $p_d = 0.2$ and varying $\tau_r = 0.5$, 1.0, and, 2.0 s. The means from 25 runs for τ_v, τ_r, and p_d are plotted with $\pm\sigma$ uncertainty brackets for each combination of τ_r and number of visit cycles.

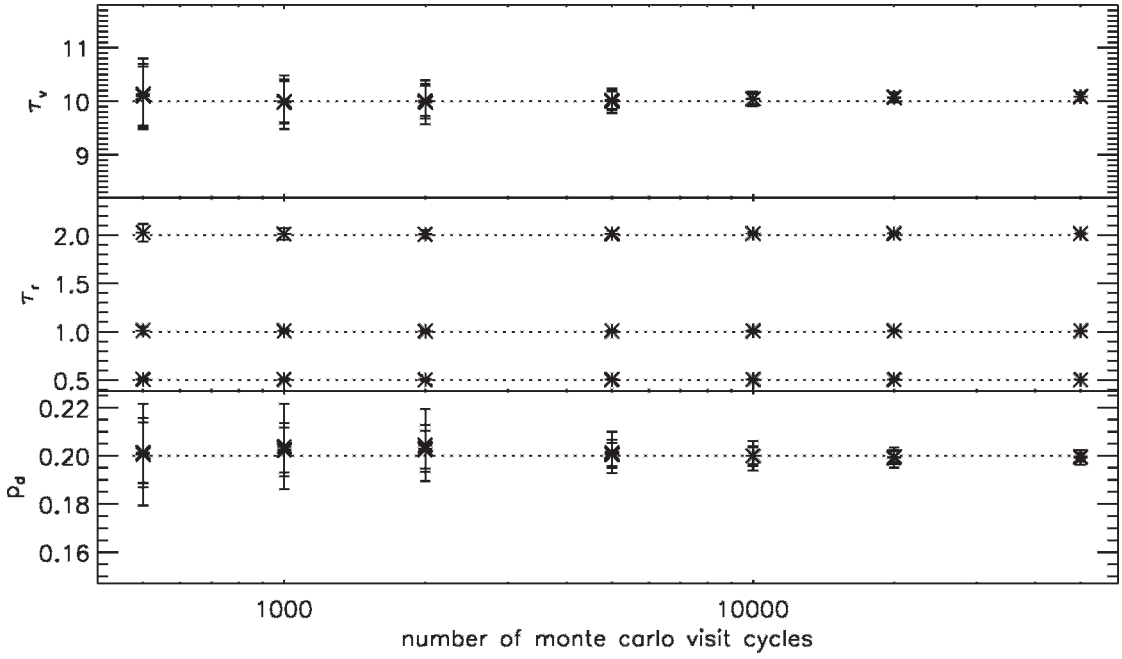

Fig. 8. Monte Carlo convergence tests of Equation 28's fit of $\mathrm{surv}_{\mathrm{IRT}}$ with fixed values of $\tau_v = 10.0$ s and $p_d = 0.2$ and varying $\tau_r = 0.5$, 1.0, and, 2.0 s. The means from 25 runs for τ_v, τ_r, and p_d are plotted with $\pm\sigma$ uncertainty brackets for each combination of τ_r and number of visit cycles.

EXTENDING THE MODEL TO INCLUDE A REFRACTORY PERIOD

For 500 visit-cycle Monte Carlo runs with $\tau_v = 10.0$ s, and $\tau_r = 0.5$ s, and $p_d = 0.2$, the shortest IRT out of the roughtly 2,500 generated is approximately 0.0002 s (or 0.2 ms). The shortest IRT in Killeen's (2003) Excel spreadsheet example is also about 0.2 ms. Clearly, such IRT values are multiple hundreds of times faster than physically possible. In the Shull, Grimes, and Bennett (2004) rat data in Figure 5 the shortest IRT is 70 ms. Consequently, a more behaviorally reasonable model would cut off the short end the IRT distribution by requiring a refractory, or minimum, period between responses. The changes needed to extend the basic Shull et al. (2001) model to accommodate a refractory cutoff are minimal.

Using Killeen's (2002) notation of δ for this refractory cut-off, Equations 1 and 2 change

$$p_v(t) = \frac{1}{\tau_v} e^{(t-\delta)/\tau_v} \Theta(t-\delta) \tag{31}$$

and

$$p_r(t) = \frac{1}{\tau_r} e^{(t-\delta)/\tau_r} \Theta(t-\delta) \tag{32}$$

The $\Theta(t-\delta)$ is the step function given by

$$\Theta(t-\delta) = \begin{cases} 0 & t < \delta \\ 1 & t > \delta \end{cases}. \tag{33}$$

The probabilistic switching is unchanged, so Equations 12, 13, and 14 remain valid. Consequently, the overall IRT probability density function when one includes a refractory period is

$$p_{\text{IRT}}(t;\tau_v,\tau_r,p_d,\delta) = \frac{p_d}{\tau_v} e^{-(t-\delta)/\tau_v} \Theta(t-\delta) + \frac{1-p_d}{\tau_r} e^{-(t-\delta)/\tau_r} \Theta(t-\delta). \tag{34}$$

which follows immediately upon substitution of the right sides of Equations 31, 32, 12, and 13 into Equation 14. Equation 34 integrates promptly to

$$P_{\text{IRT}}(t_1,t_2;\tau_v,\tau_r,p_d,\delta) = \int_{t_1}^{t_2} p_{\text{IRT}}(t;\tau_v,\tau_r,p_d,\delta)\,dt, \tag{35}$$

$$= \begin{cases} 0 & t_1,t_2 < \delta \\ p_d\left[1 - e^{-(t_2-\delta)/\tau_v}\right] + (1-p_d) \times \left[1 - e^{-(t_2-\delta)/\tau_r}\right] & t_1 < \delta \le t_2 \\ p_d\left[e^{-(t_1-\delta)/\tau_v} - e^{-(t_2-\delta)/\tau_v}\right] + (1-p_d)\left[e^{-(t_1-\delta)/\tau_r} - e^{-(t_2-\delta)/\tau_r}\right] & \delta \le t_1,t_2 \end{cases} \tag{36}$$

as the analog of Equation 17. Similarly, the survivor fraction with a refractory period follows immediately as

$$\text{surv}_{\text{IRT}}(t;\tau_v,\tau_r,p_d,\delta) = \int_t^{\infty} p_{\text{IRT}}(t';\tau_v,\tau_r,p_d,\delta)\,dt', \tag{37}$$

$$= \begin{cases} 1 & t < \delta \\ p_d\, e^{-(t-\delta)/\tau_v} + (1-p_d)e^{-(t-\delta)/\tau_r} & \delta \le t \end{cases}. \tag{38}$$

The reduced chi-square expression for a weighted least-squares estimate using the Equation 38 survivor fraction is

$$\chi^2_\nu = \frac{1}{N-4}\left[\sum_{\widehat{\text{surv}}_{\text{IRT}}(t_i) < \delta} \frac{1}{\sigma^2_{\text{surv}_{\text{IRT}_i}}} \left(\widehat{\text{surv}}_{\text{IRT}}(t_i) - 1\right)^2 + \sum_{\widehat{\text{surv}}_{\text{IRT}}(t_i) \ge \delta} \frac{1}{\sigma^2_{\text{surv}_{\text{IRT}_i}}} \left(\widehat{\text{surv}}_{\text{IRT}}(t_i) - p_d\, e^{-(t-\delta)/\tau_v} - (1-p_d)e^{-(t-\delta)/\tau_r}\right)^2\right], \tag{39}$$

Note the change in degrees of freedom to $\nu = N - 4$ with the addition of the δ parameter. Inclusion of a refractory period yields the dashed-dot fit shown in Figure 5. The fit does more closely follow the measured distribution for the shortest IRT values and the χ^2_ν improves. However, the F_χ test of an additional term (Bevington and Robinson, 2002, pp. 207–208) yields a value of 0.277 for the IRT distribution which is well short of the 3.98

cutoff value at $v = 71$ and the 95% confidence limit required for the refractory period to significantly improve the fit. This is reasonable since Rat C1's refractory period appears to affect only the shortest and perhaps second shortest bin in the distribution.

EXTENDING THE MODEL FOR STRONGLY-BANDED PIGEON BEHAVIOR

Palya (1992) showed that pigeons have a strong banding in their IRT distribution. This is a quite different temporal structure for responses than that seen for the rats' nose pokes or lever presses studied in Shull et al.'s (2001) experiments. The left panel in Figure 9 shows the IRT population for Pigeon 694 from Bowers et al. (2003, 2008) when responding on a VI 60-s schedule plotted in the dot plot form developed by Palya. For this particular pigeon, there is a clearly visible band centered at an IRT value of 0.1 s (often colloquially labeled a ''nibble'' band). The pigeon's main band peaks at an IRT value of 0.3 s. Very weak double and triple period bands are discernible with centers of approximately 0.75 s and 1.0 s. Other pigeons in the study have similar banding structures, though the main band's precise period as well as relative strengths of the nibble and double and triple period bands are distinctive characteristics unique to each individual. For the current undertaking of extending Shull et al.'s model into strongly banded behavior, a qualitative understanding of the temporal structure is sufficient. Readers interested in more quantitative properties of banded behavior should study original articles by Palya and coworkers (Palya, 1992; Bowers et al., 2003, 2008).

The right panel in Figure 9 shows Pigeon 694's IRT histogram plotted in semilog coordinates. The histogram is formed by sweeping all IRTs spread along the left panel's time-in-interval axis into a set of equal-width bins and recording their number. The dot plot's bands appear in the histogram as local maxima. The histogram also has a clear exponential decay for the IRT values longer than about 1.3 s. As noted at the outset of the analytic development, cf. Equation 1, an IRT distribution that limits to an exponential decay for long IRT values is the indicative of a uniform-in-time random visit-initiation process.

There are important differences between the Bowers et al. (2003, 2008) data and Shull et al.'s (2001) results. The foremost difference, provided that the exponential decay is the visit-initiation IRT population, is that the time scale difference compared to the within-bout IRT population is significantly smaller than for the rat behavior observed by Shull et al. If such a smaller time scale difference had obtained for Shull et al.'s rats, it would produce something akin to the $\tau_r = 2.0$ case shown in the top panels of Figures 3 and 4. Further, if the pigeons' behavior were exactly analogous to the rats, save for their high-rate within-bout responding being banded, then the visit-initiation population would extend across the entire histogram. Graphically, this would mean that banded behavior in Figure 9 would rest on top of a background visit-initiation response population. The dashed curve (labeled ''exact analog'') extending from the exponential fit above the obtained IRT histogram is the form expected if the pigeon's visit-initiation process were an exact analog to the one that governs Shull et al.'s observations with rats.

There are at least two ways to treat the differences between the Bowers et al. (2003, 2008) observations and the original Shull et al. (2001) observations while retaining the basic character of Shull et al.'s model. The first approach is to introduce a minimum time cutoff specific to the visit-initiation IRT distribution; in essence, to model the visit-initiation responding as having a unique refractory period that is longer than most if not all of the within-bout responding. This differs from the refractory modeling for the rat behavior where the common δ cuts off the short end of both the visit-initiation IRTs in Equation 31 and the within-bout IRTs in Equation 31. The histogram panel in Figure 9 shows a possible refractory cut-off to the visit-initiation IRT distribution with the dashed curve (labeled ''cut-off'') that falls quickly for IRT values less than 1.1 s. To some extent the use of a refractory cut-off is the same approach as existed prior to Shull et al.'s 2001 article — one splits the IRT population at a fixed time and assigns all shorter IRTs to within-bout behavior and all longer IRTs to visit-initiation behavior. That subset of Bowers et al.'s data shown in Figure 9 suggests that such a split is possible for some pigeons. Functionally, a refractory cut-off means that once Pigeon 694

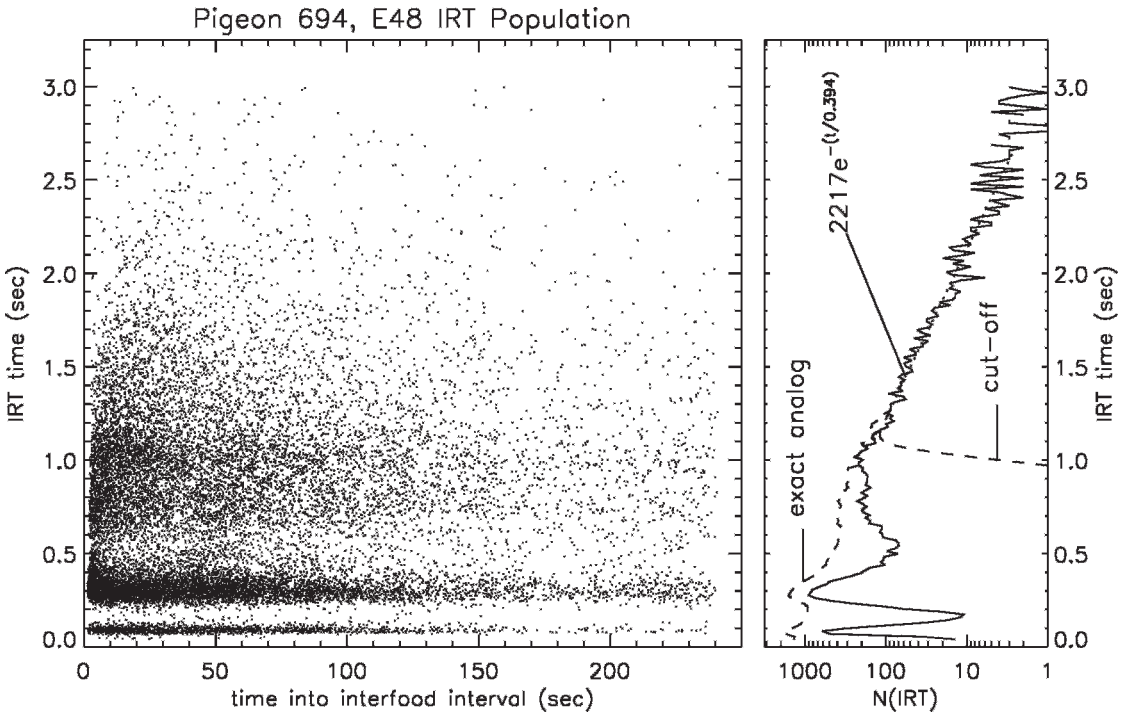

Fig. 9. Dot plot for Pigeon 694's IRT population during E48 at JSU (left panel). IRT histogram from the same data set (right panel). The dotted line is a decaying exponential fit in semilog coordinates to the histogram values over the range 1.3 to 2.65 s. The dashed curve extending from the exponential fit above the obtained IRT histogram is the form expected if the pigeon's visit-initiation process has no refractory cut-off. The dashed curve falling away quickly fromthe exponential fit beneath the data shows a visit-initiation process with a refractory cut-off of 1.3 s.

disengages from a response bout, the shortest visit-initiation IRT on this schedule is longer than at least a couple of multiples of the main band period. For some of Bowers et al.'s other pigeons, the IRT distribution extends to values longer than the 3 s of Figure 9 and has a significantly shallower slope in semi-log coordinates. For these pigeons one could justifiably treat the entire banded region plus the initial steeper exponential decay as the high rate within-bout responding and recover a complicated analog to the rats' behavior. It appears that pigeons can generate behavior that agrees with either of these two explanations as well as an extensive set of intermediate cases depending on the specific bird and schedule parameters in effect. For a full consideration of the pigeons' behavior, see the article by Bowers, Hill, and Palya (2008).

While both explanations are reasonable, we will focus on use of a refractory cutoff in the visit-initiation IRT distribution. It will turn out that most of the intermediate behaviors seen by Bowers et al. (2008) can be readily understood using this approach. Appendix C describes the details for a Monte Carlo simulation that closely parallels the one already developed from Equations 1, 2, and 6. The major difference between the two Monte Carlo simulations is the substitution of a new pair of probability density functions appropriate to the pigeon's within-bout and visit-initiation responding. These substitutions do preclude simple closed-form expression like Equations A-1 and A-2 for the cumulative probabilities. This is a minor matter as numerical remapping can provide the equivalent function.

Reasonable pairs of IRT probability density functions, analogs for Equations 1 and 2, for Pigeon 694's visit-initiation and within-bout responding are suggested by the IRT histogram replotted in Figure 10's top panel. These analogs have more intricate forms than is required for the rats and the within-bout responding will be defined by a numerical table. It is also important to note that the pigeon IRT probability density functions provide something a bit closer to an

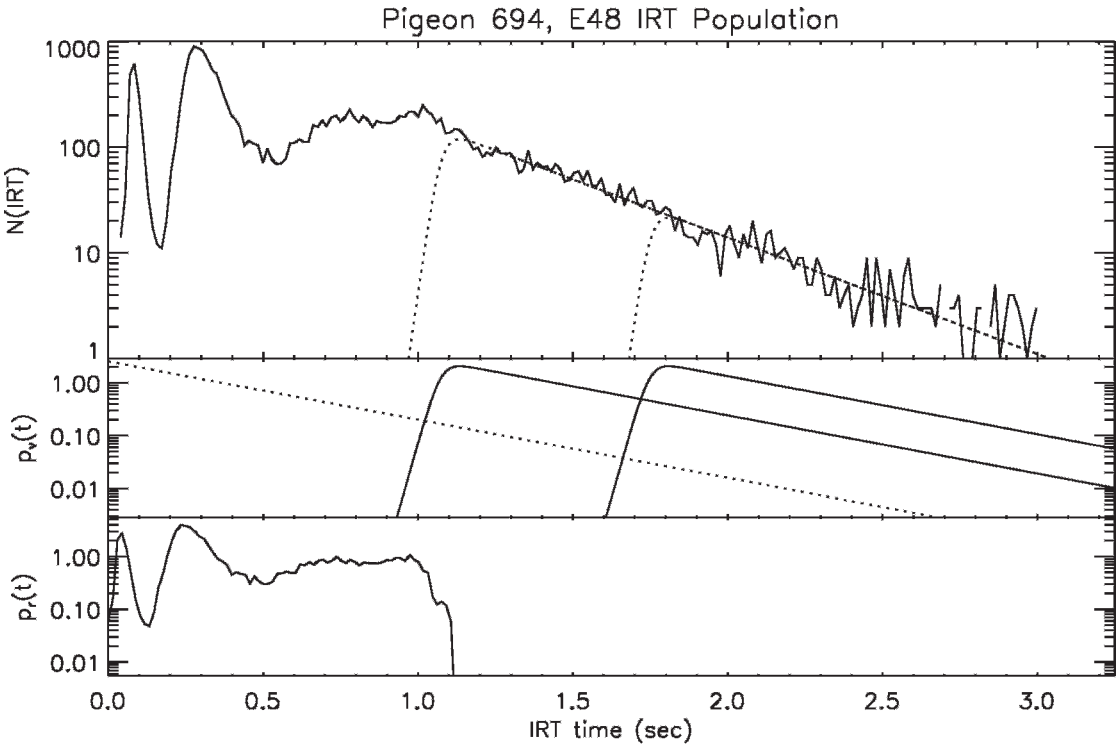

Fig. 10. IRT histogram for Pigeon 694 during E48 at JSU (top panel). The heavy dotted line is a decaying exponential fit in semilog coordinates to the histogram values over the range 1.3 to 2.65 s. The light dotted curve that coincides with the complete decaying exponential fit and falls away at about 1.1 s is a cut-off visit-initiation model that will reasonably match the data. The light dotted curve that falls away at about 1.7 s is a second cut-off visit-initiation model that generates an intermediate case. Normalized visit-initiation $p_v(t)$ models with t_{cut} of 1.075 s and 1.75 s, $m_{\text{cut}} = 25$, and $\tau = 0.394$ s (middlepanel). Also shown in the middle panel as a dotted line is the normalized visit initiation density given by Equation 1 for $\tau_v = 0.394$ s. A normalized strongly banded within-bout $p_r(t)$ model for Pigeon 694 is shown in the bottom panel.

illustration, rather than the rigorous result obtained above for the rats' behavior. The pigeons' behavior is sufficiently more complex that to include a complete description at the outset would obscure how a modified form of the Shull et al.'s (2001) model operates. With these provisos in mind, we will first attend to the visit-initiation probability density function.

As noted above, the transition in IRT distribution from banded to an exponential decay near 1.3 s can be treated as a boundary between visit-initiation and within-bout responding. As a model for a somewhat soft boundary, we will use the hyperbolic tangent to generate a refractory cut-off for the visit-initiation responding as

$$\text{cut\_off}(t) = \frac{1}{2}[\tanh[m_{\text{cut}}(t - t_{\text{cut}})] + 1], \quad (40)$$

where m_{cut} is the cut-off slope and t_{cut} is the refractory cut-off time. Equation 40 is merely a convenient form that changes smoothly from 0 to 1 with half-way point centered at t_{cut}. Within Equation 40, t_{cut} plays exactly the same role as δ plays Equation 33. Considerable further experimental study will likely be required before a model for the short portion of pigeons' visit-initiation IRT distribution gains general acceptance. The long IRT portion of the distribution, on the other hand, clearly remains a simple exponential decay, as was seen in Shull et al.'s (2001) rats. Hence, a reasonable overall visit-initiation IRT distribution takes the form

$$p_v(t) = \frac{1}{2\mathcal{N}}[\tanh[m_{\text{cut}}(t - t_{\text{cut}})] + 1] \frac{1}{\tau_v} \times e^{-t/\tau_v}, \quad (41)$$

where $\mathcal{N}$ is a normalization constant. Equation 41 is the pigeon analog to Equation 1 for the rats. The middle panel of Figure 10 shows two examples of Equation 41 – one with the cutoff placed just beyond the banded behavior and one with cutoff well separated from the banded behavior.

As noted (Bowers et al. 2003, 2008; Palya, 1992), while the bands of the within-bout behavior have features common to most pigeons, their timing and relative strength are unique to the individual. Furthermore, a closed form expression for the within-bout IRT probability density function is not currently available. However, one can always subtract off Equation 41 and treat the remaining population as a numerical estimate of the within-bout probability density function. The bottom panel of Figure 10 shows such a $p_r(t)$ estimate for Pigeon 694 after it has been normalized to $\int p_r(t) = 1$. Like the use of Equation 40 as a factor in $p_v(t)$, this estimate for the within-bout probability density function will likely be superseded with further experimental work. For the present though, a numerical estimate is adequate for coding a Monte Carlo simulation. One does have to assert an additional property for the pigeons' $p_r(t)$ that parallels a property seen with the rats: its form remains fixed independent of both the visit-initiation probability density function $p_v(t)$ and the disengagement probability p_d.

Figure 11 shows the Monte Carlo's IRT output sorted into both a semilog IRT histogram and the equivalent survivor-fraction assuming five different visit-initiation patterns. The within-bout behavior is the same for all examples: the $p_r(t)$ abstracted from Pigeon 694's banded behavior shown in the bottom panel of Figure 10. All five Monte Carlo runs used 250,000 simulation cycles. The top four cases all have $p_d = 0.2$, while the fifth row used $p_d = 0.6$. The top row's pair of plots result from a cutoff $p_v(t)$ estimated for Pigeon 694 with $t_{\text{cut}} = 1.075$ s, $m_{\text{cut}} = 25$, and $\tau_v = 0.394$ s. Since this parameter set comes directly from the Pigeon 694 data, not surprisingly, the Monte Carlo generated IRT histogram agrees closely with that from the actual data. The corresponding log-survivor plot has a somewhat stair step appearance with inflection points tied to the strong band edges for IRT values below t_{cut} and the relatively straight decay for longer IRT values. Since Pigeon 694's within-bout and visit-initiation behavior have relatively similar characteristic time scales, the sharp demarcation present for the rats' log survivor plot is not apparent. Expressed quantitatively, a typical pigeon's within-bout IRT from Bowers et al.'s (2008) experiment appears to be about 3 times faster than a visit-initiation IRT, while Shull et al.'s (2001) data suggests a factor of 20 is typical for the behavior of rats under the conditions studied. The second row's pair of plots illustrates the effect of completely separating the visit-initiation responding from the within-bout responding by increasing t_{cut} to 1.75 s (shown as the right-most $p_v(t)$ in the middle panel of Figure 10). The result is a prominent split in the IRT histogram (left-hand plot) and a corresponding completely flat section in the log survivor plot (right-hand plot). Such a separation has been seen by Bowers et al. (2003, 2008) on relative rich schedules. On their richest schedules the experimentally measured separation appears to be two or three times that shown in Figure 11's second row. The third and fourth rows in Figure 11 show the result of switching from Equation 41 back to Equation 1 for $p_v(t)$ while keeping the strongly banded within-bout responding for $p_r(t)$. Consequently, these two cases are closer analogs to Shull et al.'s original model for rats.

It is important to understand how features that appear in the 50,000 cycle simulation log survivor plot in Figure 6 (or Shull et al.'s (2001) original plots) are tied to those in the bottom two rows of Figure 11. It is easier to see the connections by working in from the right, or longer IRT, side of the plots. The longest IRT population is due to visit initiations and is a straight line in all cases. The first concave upward rise (at about 1 s) from the right is the transition to contributions from the within-bout responding. For the third and fourth rows of Figure 11 this transition is at 1 s. The transition is also at 1 s in Figure 6, though it is a little difficult to see given the larger range of the axis. Once the transition occurs, the differences in the within-bout responding become important. The rats' log-survivor plots have a simple near-linear rise below the curved transition region. This inner near-linear rise is primarily the within-bout response population with just a small contribution from the very shortest of the visit-initiation IRTs. Since the rats' within-bout responding is distributed

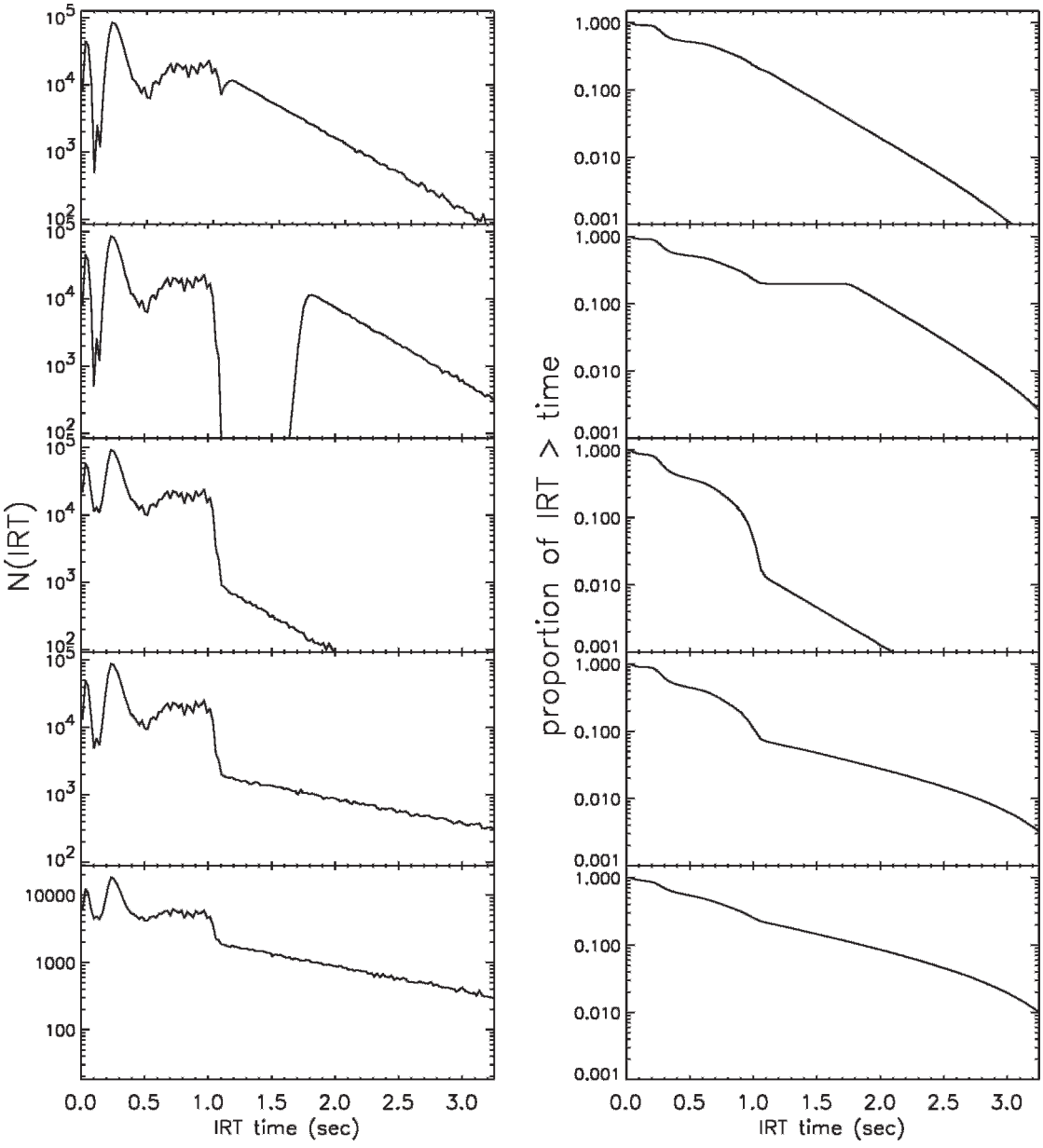

Fig. 11. IRT histograms in semilog coordinates and log survivor plots from five Monte Carlo simulations all using a 250,000 cycle run length. All cases use Pigeon 694's banded behavior shown in the bottom panel of Figure 10. The top pair of plots use cut-off visit initiation with $t_{cut} = 1.075$ s, $m_{cut} = 25$, and $\tau_v = 0.394$ s. The second row plots use cut-off visit initiation with $t_{cut} = 1.75$ s, $m_{cut} = 25$, and $\tau_v = 0.394$ s. The third, fourth, and fifth rows plots use Shull et al.'s (2001) expression for visit initiation, $(1/\tau_v)e^{-t/\tau_v}$ with: $\tau_v = 0.394$ s (third row), $\tau_v = 0.789$ s (fourth row), and $\tau_v = 0.789$ s as well as increasing p_d to 0.6 (fifth row).

uniformly in time (i.e. IRTs follow Equation 2), the associated section of the log survivor plot is a smooth rise. The pigeons' log survivor plot, in contrast, has a series of ripples caused by the band edges. Further, the time scale difference between the visit-initiation and within-bout responding is much smaller for the strongly-banded pigeon behavior than the uniformly-in-time-distributed rat behavior. Consequently, the single concave upwards change in slope in Figure 6 is comparatively much closer to the left edge of

the plot. The fourth row results from doubling τ_v to 0.789 s. The larger τ_v redistributes the visit-initiation population to greater IRT values and starts to make the strongly banded log survivor plot look more like those of the original Shull et al. model. Clearly though, the presence of strong banding will preclude the resemblance from becoming exact.

The final row in Figure 11 shows the effect of increasing to $p_d = 0.6$ while holding τ_v at 0.789 s. Both the concave upwards change in slope and the ripples from the band edges are much less apparent in the log survivor plot. Had the simulation's run length been constrained to a few thousand cycles, rather than the experimentally impractical 250,000 cycles shown in Figure 11, the small ripples present would be lost in the random fluctuations of the histogram binning.

Traversing Figure 11 captures an abbreviated characterization of the behaviors seen in Bowers et al.'s experiments (2003, 2008). Generally, as Bowers et al.'s birds were moved from lean schedules to rich schedules, their behavior shifts from larger values of p_d towards smaller values. On the leanest schedules, the supported behavior yields relatively undifferentiated log survivor plots similar to the bottom row of Figure 11. On slightly richer schedules, the birds first go to lower values of p_d and then shorter visit-initiation τ_v distributions (e.g. fourth and third row of Figure 11 respectively). Next, the visit-initiation IRT population begins to show a lower cutoff just longer than the strongly-banded within-bout behavior as shown in the first row of Figure 11. Finally, the very richest schedules generate visit-initiation IRT values that are significantly separated from the strong banded within-bout behavior (e.g. second row of Figure 11). The type of schedule also exerts control upon IRT distribution. The companion article by Bowers et al. (2008) has a complete atlas of IRT plots. As an aside, when contrasted to Shull et al.'s (2001) data, the more complex fine structure of the pigeons' behavior may well be easier to understand with the semi-log IRT histogram than with the log-survivor plot.

SUMMARY

Constructing an analytic version of Shull et al.'s (2001) model is useful in a variety of ways. The model's characteristics can be studied in detail and the analytic form itself can be used for improved data analysis techniques. It also allows one to extend the model to behavior where the interpretation of a log-survivor plot is a bit problematic. Independent of the specific analytic form presented in this article, it is important for the reader to note that the log-survivor analysis is separate from Shull et al.'s model. Their model, based on probabilistic cycling between a high rate within-bout and lower rate visit-initiation responding, is quite general. The log-survivor plot, on the other hand, is probably at its most useful for the case of rats where $\tau_v \gg \tau_r$. In a case such as Bowers et al.'s (2003, 2008) experiments, a semilog IRT histogram will probably be more useful.

The analytic form illuminates aspects of Shull et al.'s (2001) model. In its original formulation, it is built solely from a pair of unchanging IRT distributions and the switching probability p_d. As such, it is an inspired approximation for steady state behavior, rather than the final answer for IRT distributions. We expect the model to fail for behavior that lacks continuous time symmetry (e.g. behavior supported with short repeated trials). Additionally, the use of a time-averaged log-survivor plot (or a semilog IRT histogram) throws away the sequential dependencies present in Shull et al.'s model. These sequential dependencies will need to be included in dynamic models of behavior. It is possible to construct conditional statistics that are sensitive to various sequential dependencies. One could find experimentally-testable expressions for such conditional statistics with appropriate analogs to the calculation for Equation 15 based on Equations 1, 2, and 6. As an example, one could compute the expected distributions for return maps as a function of τ_v, τ_r, and p_d.

REFERENCES

Bevington, P. R., & Robinson, D. K. (2002). *Data Reduction and Error Analysis for the Physical Sciences, Third Edition* (pp. 39–45 & 207–208). New York: McGraw-Hill.

Bowers, M. T., Zimmermann, B. Y., & Palya, W. L. (2003). Feedback functions effects in the recurrent regime of IRT distributions. Presented at the annual conference of the Association for Behavior Analysis, San Francisco, California. Available from /www.jsu.edu/depart/psychology/sebac/Feedback/.

Bowers, M. T., Hill, J. C., & Palya, W. L. (2008). Interresponse time structures in variable-ratio and variable-interval schedules. *Journal of the Experimental Analysis of Behavior, 90,* 345–362.

Enge, R. A. (1963). *Introduction to Nuclear Physics* (pp. 233–234). Reading, Massachusetts: Addison-Wesley.

Killeen, P. R. (2003). RT_Analyses_v1.3_.xls [EXCEL data analysis spreadsheet]. Retrieved September 18, 2006 from /www.asu.edu/clas/psych/research/sqab/.

Killeen, P. R., Hall, S. S., Reilly, M. P., & Kettle, L. L. (2002). Molecular analyses of the principal components of response strength. *Journal of the Experimental Analysis of Behavior, 78,* 127–160.

Palya, W. L. (1992). Dynamics in the fine structure of schedule-controlled behavior. *Journal of the Experimental Analysis of Behavior, 57,* 267–278.

Peirce, B. A. (1929). *A Short Table Of Integrals* (p. 89). Boston: Ginn and Company, 89, no. 758.

Press, W. H., Flannery, B. P., Teukolsky, S. A., & Vetterling, W. T. (1996). *Numerical recipes in FORTRAN 77: The art of scientific computing second edition* (pp. 675–683), Cambridge: Cambridge University Press.

Shull, R. L. (2004). Bouts of responding on variable-interval schedules: Effects of deprivation level. *Journal of the Experimental Analysis of Behavior, 81,* 155–167.

Shull, R. L., Gaynor, S. T., & Grimes, J. A. (2001). Response rate viewed as engagement bouts: Effects of relative reinforcement and schedule type. *Journal of the Experimental Analysis of Behavior, 75,* 247–274.

Shull, R. L., Gaynor, S. T., & Grimes, J. A. (2002). Response rate viewed as engagement bouts: Resistance to extinction. *Journal of the Experimental Analysis of Behavior, 77,* 211–231.

Shull, R. L., & Grimes, J. A. (2003). Bouts of responding from variable-interval reinforcement of lever pressing by rats. *Journal of the Experimental Analysis of Behavior, 80,* 159–171.

Shull, R. L., Grimes, J. A., & Bennett, J. A. (2004). Bouts of responding: The relation between bout rate and the rate of variable-interval reinforcement. *Journal of the Experimental Analysis of Behavior, 81,* 65–83.

Received: October 30, 2007
Final Acceptance: July 31, 2008

APPENDIX A

The nice time-sequential structure of the Shull et al. (2001) model seen in Figure 2 makes it particularly convenient for computer simulation. The steps of the Monte Carlo simulation itself are a matter of iterating cycles through Shull et al.'s state diagram while satisfying Equations 1, 2, and 6 and collecting a simulated IRT set. Each of the steps involves remapping of a random number uniformly distributed between 0 and 1 to the appropriate distribution defined by Equations 1, 2, or 6.

Assuming that the organism just started a bout of responding, the simulation's basic structure follows:

1. Get number of responses in a bout. Equation 6 gives the probability for a bout of exactly n responses. Consequently $\sum_{n'=1}^{n} p_e(n')$ is the cumulative probability of n or fewer responses in a bout and is shown in Figure A-1 for $p_d = 0.2$ out to a bout of 50 responses. If all values of a uniformly-distributed pseudo-random number u within the range of $\sum_{n=1}^{n'-1} p_{n_r\, n}$ and $\sum_{n=1}^{n'} p_{n_r\, n}$ are mapped to a bout with n' responses, the number of responses in each bout length will be distributed as Equation 6. For an example of this mapping, assume that $p_d = 0.2$ and a call to a uniform random number routine yields $u = 0.716949$. As shown in Figure A-1, this is between 0.672320 and 0.737856 which are the cumulative probabilities for $n = 5$ and $n = 6$ respectively. Hence, $u = 0.716949$ corresponds to a bout with six responses. While generating the number of responses for a bout at the outset may appear as a slight departure from the Shull et al.'s (2001) state diagram description in the sense that p_d determines the probability to end a bout after each response, it is functionally equivalent. The combined effect of multiple probabilistic decisions to possibly end a bout each with probability p_d yields Equation 6.
2. Generate the within-bout IRT set. If there are n' responses in a bout, there need to be $n' - 1$ IRTs in the bout distributed according to Equation 2. Since Equation 2describes a continuous monotonically decreasing distribution with a simple closed form integral, the remapping process is done analytically. One equates cumulative probabilities, $\int_0^u du'$ and $\int_0^{\mathrm{IRT_{bout}}} \frac{1}{\tau_r} e^{-t'/\tau_r} dt'$, which yields an analytic expression

$$\mathrm{IRT_{bout}} = -\tau_r \ln(1 - u). \qquad \text{(A–1)}$$

Equation A-1 remaps a uniformly distributed pseudorandom number u to an $\mathrm{IRT_{bout}}$ which satisfies Equation 2's probability density. Continuing with the example of the first step where an initial random number call of $u = 0.716949$ mapped to a bout of six responses, will require five IRT values. If five calls to uniform random number routine yield the set of values

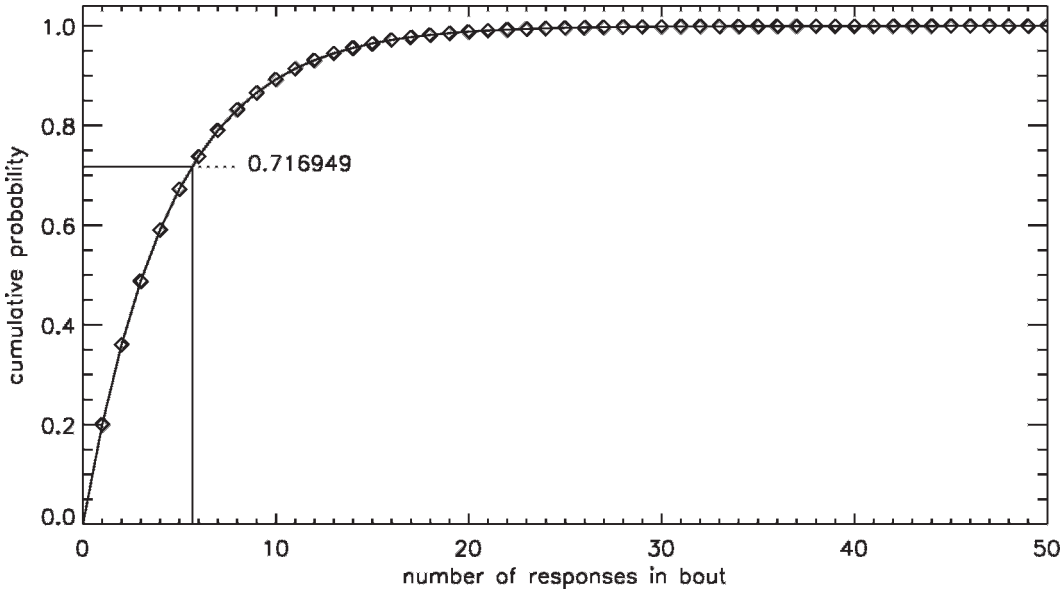

Fig. A-1. $\sum_{n=1}^{n} p_{n,\,n}$ for $p_d = 0.2$. Also shown is the remapping from $u = 0.716949$ to six responses.

{0.698975, 0.476577, 0.562559, 0.268977, 0.169790} and $\tau_r = 0.50$ then the associated IRT_{bout} values from Equation A-1 are {0.60028160, 0.32368273, 0.41340727, 0.15665530, 0.093038388}.

3. Generate the visit-initiation IRT. Since the visit-initiation IRT distribution's form is also an exponential (Equation 1), it can be handled in the same way as the within-bout distribution. The visit-initiation analog to Equation A-1 is

$$IRT_{visit} = -\tau_v \ln(1 - u). \qquad \text{(A–2)}$$

Completing the example in use for this cycle of the simulation, if the next random number call returns $u = 0.504665$ and $\tau_v = 10.0$, the associated IRT_{visit} value is 7.0252186.

The simulation then returns to Step 1 and is iterated until an IRT population for some predetermined number of cycles has been generated. In addition to generating the IRT population, the simulation also collects the IRTs into histogram bins and logs the actual numbers of within-bout and visit-initiation IRTs.

APPENDIX B: PARTIAL DERIVATIVES WITH RESPECT TO MODEL PARAMETERS

The Levenberg-Marquardt algorithm uses the partial derivatives of the function to be fit with respect to each of the adjustable parameters. For completeness, the partial derivatives used for this article's fits follow below.

The partials of Equation 17 are:

$$\frac{\partial P_{IRT}(t_1,t_2;\tau_v,\tau_r,p_d)}{\partial \tau_v} = \frac{p_d}{\tau_v^2}\left[t_1 e^{-t_1/\tau_v} - t_2 e^{-t_2/\tau_v}\right], \qquad \text{(B–1)}$$

$$\frac{\partial P_{IRT}(t_1,t_2;\tau_v,\tau_r,p_d)}{\partial \tau_r} = \frac{1 - p_d}{\tau_r^2}\left[t_1 e^{-t_1/\tau_r} - t_2 e^{-t_2/\tau_r}\right], \qquad \text{(B–2)}$$

and

$$\frac{\partial P_{IRT}(t_1,t_2;\tau_v,\tau_r,p_d)}{\partial p_d} = \left[e^{-t_1/\tau_v} - e^{-t_2/\tau_v}\right] - \left[e^{-t_1/\tau_r} - e^{-t_2/\tau_r}\right]. \qquad \text{(B–3)}$$

The partials of Equation 19 are

$$\frac{\partial \,\mathrm{surv}_{\mathrm{IRT}}(t;\tau_v,\tau_r,p_d)}{\partial\,\tau_v} = \frac{p_d}{\tau_v^2}e^{-t/\tau_v}, \qquad \text{(B–4)}$$

$$\frac{\partial \,\mathrm{surv}_{\mathrm{IRT}}(t;\tau_v,\tau_r,p_d)}{\partial\,\tau_r} = \frac{1-p_d}{\tau_r^2}e^{-t/\tau_r}, \qquad \text{(B–5)}$$

and

$$\frac{\partial \,\mathrm{surv}_{\mathrm{IRT}}(t;\tau_v,\tau_r,p_d)}{\partial\,p_d} = e^{-t/\tau_v} - e^{-t/\tau_r}, \qquad \text{(B–6)}$$

The partials of Equation 36 are

$$\frac{\partial\, P_{\mathrm{IRT}}(t_1,t_2;\tau_v,\tau_r,p_d,\delta)}{\partial\,\tau_v} = \begin{cases} 0 & t_1,t_2 < \delta \\ -p_d\, e^{-(t_2-\delta)/\tau_v}\left(\frac{t_2-\delta}{\tau_v^2}\right) & t_1 < \delta \le t_2 \\ p_d\left[e^{-(t_1-\delta)/\tau_v}\left(\frac{t_1-\delta}{\tau_v^2}\right)\right. & \\ \left. -\ e^{-(t_2-\delta)/\tau_v}\left(\frac{t_2-\delta}{\tau_v^2}\right)\right] & \delta \le t_1,t_2 \end{cases}, \qquad \text{(B–7)}$$

$$\frac{\partial\, P_{\mathrm{IRT}}(t_1,t_2;\tau_v,\tau_r,p_d,\delta)}{\partial\,\tau_r} = \begin{cases} 0 & t_1,t_2 < \delta \\ -(1-p_d)e^{-(t_2-\delta)/\tau_r}\left(\frac{t_2-\delta}{\tau_r^2}\right) & t_1 < \delta \le t_2 \\ (1-p_d)\left[e^{-(t_1-\delta)/\tau_r}\left(\frac{t_1-\delta}{\tau_r^2}\right)\right. & \\ \left. -\ e^{-(t_2-\delta)/\tau_r}\left(\frac{t_2-\delta}{\tau_r^2}\right)\right] & \delta \le t_1,t_2 \end{cases}, \qquad \text{(B–8)}$$

$$\frac{\partial\, P_{\mathrm{IRT}}(t_1,t_2;\tau_v,\tau_r,p_d,\delta)}{\partial p_d} = \begin{cases} 0 & t_1,t_2 < \delta \\ \left[1-e^{-(t_2-\delta)/\tau_v}\right] & \\ \quad -\left[1-e^{-(t_2-\delta)/\tau_r}\right] & t_1 < \delta \le t_2, \\ \left[e^{-(t_1-\delta)/\tau_v} - e^{-(t_2-\delta)/\tau_v}\right] & \\ \quad -\left[e^{-(t_1-\delta)/\tau_r} - e^{-(t_2-\delta)/\tau_r}\right] & \delta \le t_1,t_2 \end{cases} \qquad \text{(B–9)}$$

and

$$\frac{\partial\, P_{\mathrm{IRT}}(t_1,t_2;\tau_v,\tau_r,p_d,\delta)}{\partial\delta} = \begin{cases} 0 & t_1,t_2 < \delta \\ -\left\{p_d e^{-(t_2-\delta)/\tau_v}\left(\frac{1}{\tau_v}\right)\right. & \\ \left. +\ (1-p_d)e^{-(t_2-\delta)/\tau_r}\left(\frac{1}{\tau_r}\right)\right\} & t_1 < \delta \le t_2 \\ p_d\left[e^{-(t_1-\delta)/\tau_v}\left(\frac{1}{\tau_v}\right)\right. & \\ \quad \left. -\ e^{-(t_2-\delta)/\tau_v}\left(\frac{1}{\tau_v}\right)\right] & \\ \quad +\ (1-p_d)\left[e^{-(t_1-\delta)/\tau_r}\left(\frac{1}{\tau_r}\right)\right. & \\ \quad \left. -\ e^{-(t_2-\delta)/\tau_r}\left(\frac{1}{\tau_r}\right)\right] & \delta \le t_1,t_2 \end{cases}, \qquad \text{(B–10)}$$

$$= \begin{cases} 0 & t_1,t_2 < \delta \\ -\left\{\left(\frac{p_d}{\tau_v}\right)e^{-(t_2-\delta)/\tau_v}\right. & \\ \left. +\ \left(\frac{(1-p_d)}{\tau_r}\right)e^{-(t_2-\delta)/\tau_r}\right\} & t_1 < \delta \le t_2 \\ \left(\frac{p_d}{\tau_v}\right)\left[e^{-(t_1-\delta)/\tau_v}\right. & \\ \quad \left. -\ e^{-(t_2-\delta)/\tau_v}\right] & \\ \quad +\ \left(\frac{(1-p_d)}{\tau_r}\right) & \\ \quad \left[e^{-(t_1-\delta)/\tau_r} - e^{-(t_2-\delta)/\tau_r}\right] & \delta \le t_1,t_2 \end{cases}. \qquad \text{(B–11)}$$

And finally the partials for Equation 38 are

$$\frac{\partial \,\mathrm{surv}_{\mathrm{IRT}}(t_1,t_2;\tau_v,\tau_r,p_d,\delta)}{\partial\,\tau_v} = \begin{cases} 0 & t < \delta \\ p_d e^{-(t-\delta)/\tau_v}\left(\frac{t-\delta}{\tau_v^2}\right) & \delta \le t \end{cases}, \qquad \text{(B–12)}$$

$$\frac{\partial \,\mathrm{surv}_{\mathrm{IRT}}(t_1,t_2;\tau_v,\tau_r,p_d,\delta)}{\partial\,\tau_r} = \begin{cases} 0 & t < \delta \\ (1-p_d)e^{-(t-\delta)/\tau_r}\left(\frac{t-\delta}{\tau_r^2}\right) & \delta \le t \end{cases}, \qquad \text{(B–13)}$$

$$\frac{\partial \,\mathrm{surv}_{\mathrm{IRT}}(t_1,t_2;\tau_v,\tau_r,p_d,\delta)}{\partial\,p_d} = \begin{cases} 0 & t < \delta \\ e^{-(t-\delta)/\tau_v} - e^{-(t-\delta)/\tau_r} & \delta \le t \end{cases}, \qquad \text{(B–14)}$$

and

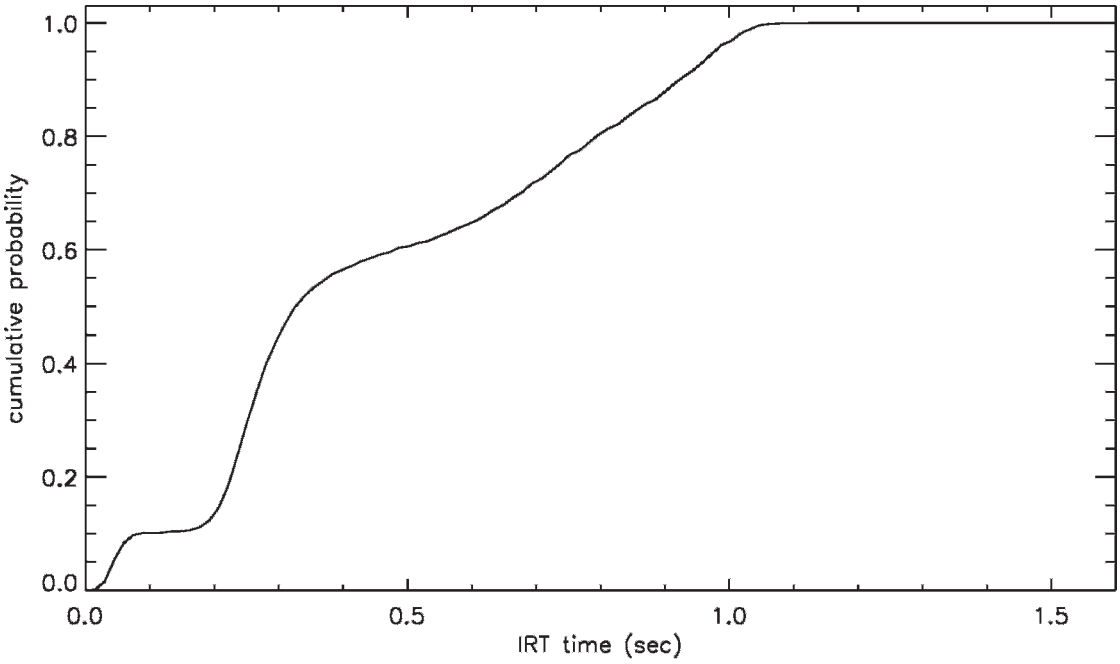

Fig. C-1. The cumulative probability from evaluating Equation C-1 for all $\mathrm{IRT}_{\mathrm{bout}}$.

$$\frac{\partial\, \mathrm{surv}_{\mathrm{IRT}}(t_1,t_2;\tau_v,\tau_r,p_d,\delta)}{\partial\,\delta} = \begin{cases} 0 & t < \delta \\ \left(\frac{p_d}{\tau_v}\right) e^{-(t-\delta)/\tau_v} + \left(\frac{(1-p_d)}{\tau_r}\right) e^{-(t-\delta)/\tau_r} & \delta \le t \end{cases} . \quad \text{(B–15)}$$

APPENDIX C: STRONG BANDING PIGEON MONTE CARLO

The pigeon Monte Carlo has nearly an identical structure to the one developed earlier for the rats. To ease the comparisons, we will again use $p_d = 0.2$ and repeat the same example set of uniformly distributed pseudo-random numbers that were used to explain the rat Monte Carlo. The steps in the pigeon Monte Carlo are:

1. Get number of responses in a bout. The first step is exactly the same as for the rat Monte Carlo simulation. Equation 6 gives the probability for a bout of exactly n responses and Figure A-1's technique still applies. Assuming that a call to uniform random number routine again yields $u = 0.716949$, a p_d of 0.2 maps to a bout of six responses.
2. Generate the within-bout IRT set. As before if there are n' responses in a bout, there need to be $n' - 1$ IRTs in the bout. However, unlike the rats' behavior, the pigeons' within-bout strongly-banded behavior is not easily describable by a closed form expression. Rather, for Pigeon 694, its strongly-banded IRT distribution is given by the numerical estimate shown plotted in the bottom panel of Figure 10. To remap a uniformly distributed pseudo-random number u to a bout IRT requires equating the cumulative probability as

$$u(\mathrm{IRT}_{\mathrm{bout}}) = \int_0^{\mathrm{IRT}_{\mathrm{bout}}} p_r(t')\,dt', \quad \text{(C–1)}$$

where $p_r(t')$ is taken from the bottom panel of Figure 10. Figure C-1 shows the cumulative probability from evaluating Equation C-1 for all $\mathrm{IRT}_{\mathrm{bout}}$. For reasons of computational speed, Equation C-1 is

repeatedly evaluated ahead of time at a closely spaced set of IRT_{bout} values to yield a table of cumulative probabilities. During a Monte Carlo simulation run itself, this table of cumulative probabilities is interpolated for a given value of u. If five calls to uniform random number routine yield the set of values {0.698975, 0.476577, 0.562559, 0.268977, 0.169790}, then the corresponding IRT_{bout} values are {0.674384, 0.313313, 0.394776, 0.243797, 0.215848}. These values put the first IRT in Pigeon 694's double period band and the remaining four IRTs in the main band.

3. Generate the visit IRT. The pigeons' visit-initiation distribution is given by Equation 41. To convert a uniformly distributed pseudorandom number u to a IRT_{visit} value is again done by equating the cumulative probability, which now takes the form

$$u = \int_0^{IRT_{visit}} \frac{1}{2\mathcal{N}} [\tanh[m_{cut}(t' - t_{cut})] + 1] \frac{1}{\tau_v} e^{-t'/\tau_v} dt'. \quad \text{(C–2)}$$

The remapping of u to IRT_{visit} is again most efficiently done by interpolating a precomputed table of closely spaced evaluations of the integral. Assuming the Monte Carlo's next random number call returns $u = 0.504665$ and that $t_{cut} = 1.075$ s, $m_{cut} = 25$, and $\tau_v = 0.394459$ s the associated IRT_{visit} value is 1.3505170.

As with the first Monte Carlo, the routine returns to Step 1 and the steps are iterated until an IRT population is accumulated for a fixed number of simulation cycles.